Adjustment of the PIF7-HFR1 transcriptional module activity controls plant shade adaptation

Sandi Paulišić, Wenting Qin, Harshul Arora Verasztó, Christiane Then, Benjamin Alary, Fabien Nogue, Miltos Tsiantis, Michael Hothorn, Jaime Martínez-García

Adjustment of the PIF7-HFR1 transcriptional module activity controls plant shade adaptation

Sandi Paulišić[1], Wenting Qin[1], Harshul Arora Verasztó[2], Christiane Then[1a], Benjamin Alary[1], Fabien Nogue[3], Miltos Tsiantis[4], Michael Hothorn[2], Jaime F. Martínez-García[1,5,6]©

[1] Centre for Research in Agricultural Genomics (CRAG), CSIC-IRTA-UAB-UB, Cerdanyola del Vallès, Campus UAB, 08193 Barcelona, Spain.

[2] Structural Plant Biology Laboratory, Department of Botany and Plant Biology, Section of Biology, University of Geneva, 1211 Geneva, Switzerland.

[3] Institut Jean-Pierre Bourgin, INRA, AgroParisTech, CNRS, Université Paris-Saclay, 78000, Versailles, France.

[4] Department of Comparative Development and Genetics, Max Planck Institute from Plant Breeding Research, 50829 Cologne, Germany.

[4] Institució Catalana de Recerca i Estudis Avançats (ICREA), 08010 Barcelona, Spain.

[5] Institute for Plant Molecular and Cellular Biology (IBMCP), CSIC-UPV, 46022 València, Spain.

[a] Current address, Department for Epidemiology and Pathogen Diagnostics, Julius Kühn-Institut, Federal Research Institute for Cultivated Plants, 38104 Braunschweig, Germany.

Running title, PIF-HFR1 role in plant shade adaptation

ABSTRACT

Shade caused by the proximity of neighboring vegetation triggers a set of acclimation responses to either avoid or tolerate shade. Comparative analyses between the shade avoider *Arabidopsis thaliana* and the shade tolerant *Cardamine hirsuta*, revealed a role for the atypical basic-helix-loop-helix LONG HYPOCOTYL IN FR 1 (HFR1) in maintaining the shade-tolerance in *C. hirsuta*, inhibiting hypocotyl elongation in shade and constraining expression profile of shade induced genes. We showed that *C. hirsuta* HFR1 protein is more stable than its *A. thaliana* counterpart, likely due to its lower binding affinity to CONSTITUTIVE PHOTOMORPHOGENIC 1 (COP1), contributing to enhance its biological activity. The enhanced HFR1 total activity is accompanied by an attenuated PHYTOCHROME INTERACTING FACTOR (PIF) activity in *C. hirsuta*. As a result, the PIF-HFR1 module is differently balanced, causing a reduced PIF activity and attenuating other PIF-mediated responses such as warm temperature-induced hypocotyl elongation (thermomorphogenesis) and dark-induced senescence. By this mechanism and that of the already-known of phytochrome A photoreceptor, plants might ensure to properly adapt and thrive in habitats with disparate light amounts.

Keywords, *Cardamine hirsuta* / HFR1 / PIFs / shade avoidance / shade tolerance.

INTRODUCTION

Acclimation of plants to adjust their development to the changing environment is of uttmost importance. This acclimation relies on the plant's ability to perceive many cues such as water, nutrients, temperature or light. Conditions in nature often involve simultaneous changes in multiple light cues leading to an interplay of various photoreceptors to adjust plant growth appropriately (Ballare & Pierik, 2017; de Wit *et al*, 2016; Fiorucci & Fankhauser, 2017; Mazza & Ballare, 2015; Pierik & Testerink, 2014). Nearby vegetation can impact both light quantity and quality. Under a canopy, light intensity is decreased and its quality is changed as the overtopping green leaves strongly absorb blue and red light (R) but reflect far-red light (FR). As a consequence, plants growing in forest understories receive less light of a much lower R to FR ratio (R:FR) than those growing in open spaces. In dense plant communities, FR reflected by neighboring plants also decreases R:FR but typically without changing light intensity. We refer to the first situation as canopy shade (very low R:FR) and the second as proximity shade (low R:FR). In general, two strategies have emerged to deal with shade: avoidance and tolerance (Gommers *et al*, 2013; Pierik & Testerink, 2014; Valladares & Niinemets, 2008). Shade avoiders usually promote elongation of organs to outgrow the neighbors and avoid light shortages, reduce the levels of photosynthetic pigments to cope to light shortage, and accelerate flowering to ensure species survival (Casal, 2013). The set of responses to acclimate to shade is collectively known as the shade avoidance syndrome (SAS). In contrast, shade-tolerant species usually lack the promotion of elongation growth in response to shade and have developed a

variety of traits to acclimate to low light conditions and optimize net carbon gain (Smith, 1982; Valladares & Niinemets, 2008).

In *Arabidopsis thaliana*, a shade avoider plant, low R:FR is perceived by phytochromes. Among them, phyA has a negative role in elongation, particularly under canopy shade, whereas phyB inhibits elongation inactivating PHYTOCHROME INTERACTING FACTORS (PIFs), members of the basic-helix-loop-helix (bHLH) transcription factor family that promote elongation growth. In particular, PIFs induce hypocotyl elongation by initiating an expression cascade of genes involved in auxin biosynthesis and signaling [e.g., *YUCCA 8* (*YUC8*), *YUC9*, *INDOLE-3-ACETIC ACID INDUCIBLE 19* (*IAA19*), *IAA29*] and other processes related to cell elongation [e.g., *XYLOGLUCAN ENDOTRANSGLYCOSYLASE 7* (*XTR7*)]. Genetic analyses indicated that PIF7 is the key PIF regulator of the low R:FR-induced hypocotyl elongation with PIF4 and PIF5 having important contributions. Indeed, *pif7* mutant responds poorly to low R:FR compared to the *pif4 pif5* double or *pif1 pif3 pif4 pif5* quadruple (*pifq*) mutants, but the triple *pif4 pif5 pif7* mutant is almost unresponsive to low R:FR (de Wit *et al*, 2016; Li *et al*, 2012; Lorrain *et al*, 2008; van Gelderen *et al*, 2018). PhyB-mediated shade signaling involves other transcriptional regulators, such as *LONG HYPOCOTYL IN FR 1* (*HFR1*), *PHYTOCHROME RAPIDLY REGULATED 1* (*PAR1*), *BIM1, ATHB4* or *BBX* factors, that either promote or inhibit shade-induced hypocotyl elongation (Bou-Torrent *et al*, 2014; Cifuentes-Esquivel *et al*, 2013; Gallemi *et al*, 2017; Roig-Villanova *et al*, 2007; Sasidharan & Pierik, 2010; Sessa *et al*, 2005; Yang & Li, 2017). HFR1, a member of the bHLH family, is structurally related to PIFs but lacks the phyB- and DNA-binding ability that PIFs possess (Galstyan *et al*, 2011; Hornitschek *et al*, 2012). HFR1

inhibits PIF activity by heterodimerizing with them, as described for PIF1 (Shi *et al*, 2013), PIF3 (Fairchild *et al*, 2000), PIF4 and PIF5 (Hornitschek *et al*, 2009), Heterodimerization with HFR1 prevents PIFs from binding to the DNA and altering gene expression. In this manner HFR1 acts as a transcriptional cofactor that modulates SAS responses, e.g. it inhibits hypocotyl elongation in seedlings in a PIF-dependent manner, forming the PIF-HFR1 transcriptional regulatory module (Galstyan *et al*, 2011).

What mechanistic and regulatory adjustments in shade signaling are made between species to adapt to plant shade is a topic that has not received much attention until now. This question has been recently addressed performing comparative analyses between phylogenetically related species. In two related *Geranium* species that showed petioles with divergent elongation responses to shade, transcriptomic analysis led to propose that differences in expression of three factors, *FERONIA*, *THESEUS1* and *KIDARI*, shown to activate SAS elongation responses in *A. thaliana*, might be part of the adjustments necessary to acquire a shade-avoiding or tolerant habit (Gommers *et al*, 2017). When comparing two related mustard species that showed divergent hypocotyl elongation response to shade, *A. thaliana* and *Cardamine hirsuta* (Hay *et al*, 2014), molecular and genetic analyses indicated that phyA, and to a lesser extent phyB, contributed to establish this divergent response. In particular, the identification and characterization of the *C. hirsuta* phyA-deficient *slender in shade 1* (*sis1*) mutant indicated that differential features of this photoreceptor in *A. thaliana* and *C. hirsuta* could explain their differential response to shade. Thus, stronger phyA activity in *C. hirsuta* wild-type plants resulted in a suppressed hypocotyl elongation response when exposed to low

or very low R:FR (Molina-Contreras *et al*, 2019). These approaches indicated that the implementation of shade avoidance and shade tolerance involved the participation of shared genetic components. They also suggest that other responses co-regulated by these shared components will be accordingly affected.

With this frame of reference, we asked whether the phyB-dependent PIF-HFR1 module was also relevant to shape the shade response habits in different plant species. We found that *C. hirsuta* plants deficient in ChHFR1 gained a capacity to elongate in response to shade. We also report that *AtHFR1* and *ChHFR1* are expressed at different levels and encode proteins with different protein stability, caused by their different binding affinities with CONSTITUTIVE PHOTOMORPHOGENIC 1 (COP1), known to affect AtHFR1 stability under shade (Pacin *et al*, 2016). We propose that adaptation to plant shade in *A. thaliana* and *C. hirsuta* relies on the PIF-HFR1 regulatory module. As PIFs regulates several other processes, we hypothesized that a set of responses co-regulated by the PIF-HFR1 module are also affected and associated with the shade-avoidance and shade-tolerant habits. After exploring this possibility, we found that thermoregulation of hypocotyl elongation and dark-induced senescence, two well-known PIF-regulated responses (Koini *et al*, 2009; Sakuraba *et al*, 2014; Stavang *et al*, 2009), are consistently affected in *C. hirsuta*.

RESULTS

HFR1 is required for the shade tolerance habit of *C. hirsuta*

First, we wanted to determine if HFR1 has a role in the shade-tolerance habit of *C. hirsuta*, i.e., whether *ChHFR1* contributes to inhibit hypocotyl elongation when this species is exposed to shade. For this purpose, we generated several *C. hirsuta* RNAi lines to downregulate *HFR1* expression (RNAi-HFR1 lines). As expected, *ChHFR1* expression was attenuated in seedlings of two RNAi-HFR1 selected lines (#01 and #21) compared to the wild type (Ch^{WT}) (Fig EV1A). When growing under white light (W) of high R:FR (>1.5), hypocotyl length of these two RNAi-HFR1 lines was undistinguishable from Ch^{WT} (Fig 1A). By contrast, under W supplemented with increasing amounts of FR (W+FR) resulting in moderate (0.09), low (0.05-0.06) and very low (0.02) R:FR (that simulated proximity and canopy shade) (Martinez-Garcia *et al*, 2014), the hypocotyl elongation of RNAi-HFR1 seedlings was significantly promoted compared to Ch^{WT}, which was unresponsive (Fig 1A).

Using CRISPR-Cas9, we obtained two mutant lines of *ChHFR1* (named *chfr1-1* and *chfr1-2*) with a single nucleotide insertion in their sequence leading to a premature stop codon (Fig EV1C). These mutants showed a non-significant decrease of *ChHFR1* expression in W-grown seedlings (Fig EV1B). Similar to the RNAi-HFR1 lines, their hypocotyls were undistinguishable from Ch^{WT} under W but elongated strongly in response to W+FR exposure (Fig 1B), showing a *slender in shade* (*sis*) phenotype. Together, we concluded that HFR1 represses hypocotyl elongation in response to shade in *C. hirsuta*.

Exposure of *A. thaliana* wild-type (At^{WT}) and Ch^{WT} seedlings to low R:FR induces a rapid increase in the expression of various direct target genes of

PIFs, including *PIF3-LIKE 1* (*PIL1*), *YUC8* and *XTR7* (Fig 1C, D) (Ciolfi *et al*, 2013; Hersch *et al*, 2014; Molina-Contreras *et al*, 2019). The shade-induced expression of these genes was significantly higher in RNAi-HFR1 and *chfr1* mutant lines compared to Ch^{WT} (Fig 1C, D), indicating that ChHFR1 might repress shade-triggered hypocotyl elongation in part by down-regulating the rapid shade-induced expression of these genes in *C. hirsuta*, as it was observed with AtHFR1 in *A. thaliana* seedlings (Hornitschek *et al*, 2009).

***HFR1* expression is higher in *C. hirsuta* than in *A. thaliana* seedlings**

To test if the lack of elongation of Ch^{WT} hypocotyls in response to shade was caused by higher levels of *ChHFR1* expression in this species, we used primer pairs that amplify *HFR1* (Fig EV2A) and three housekeeping genes (*EF1α*, *SPC25*, *YLS8*) in both species (Molina-Contreras *et al*, 2019). As expected, expression of *HFR1* was induced in shade-treated seedlings of both species, in agreement with the presence of canonical PIF-binding sites (G-box, CACGTG) in the *HFR1* promoters (Hornitschek *et al*, 2009; Martinez-Garcia *et al*, 2000) (Fig EV3A). More importantly, *ChHFR1* transcript levels were always higher than those of *AtHFR1* during the whole period analyzed (from days 3 to 7) (Fig 2). Because HFR1 is part of the PIF-HFR1 regulatory module, we next compared transcript levels of *PIF* genes in both species. *PIF7* expression was significantly lower in *C. hirsuta* than in *A. thaliana* in either W or W+FR during the period analyzed (Fig 2). By contrast, *PIF4* expression was higher in *C. hirsuta* than in *A. thaliana*, whereas that of *PIF5* was similar in both species (Fig EV2B). Together, these results indicated that whereas *HFR1* expression is enhanced, that of *PIF7* is globally attenuated in Ch^{WT} compared to At^{WT}

seedlings. As a consequence, the PIF-HFR1 transcriptional module might be differently balanced in these species, with HFR1 imposing a stronger suppression on the PIF7-driven hypocotyl elongation in the shade-tolerant *C. hirsuta* seedlings.

ChHFR1 protein is more stable than AtHFR1

A higher specific activity of ChHFR1 compared to its orthologue AtHFR1 might also contribute to the role of this transcriptional cofactor in maintaining the shade tolerance habit of *C. hirsuta*. To test this possibility, we transformed *A. thaliana hfr1-5* plants with constructs to express either *AtHFR1* or *ChHFR1* fused to the 3x hemagglutinin tag (3xHA). These genes were expressed under the transcriptional control of the 2 kb of the *AtHFR1* promoter (*pAt*), generating *hfr1>pAt:ChHFR1* and *hfr1>pAt:AtHFR1* lines (Fig 3A). Fusion of *pAt* to the *GUS* reporter gene resulted in GUS activity in cotyledons and roots of transgenic lines, with increased levels in hypocotyls of seedlings exposed for 2-4 h to W+FR (Fig EV3B). Several independent transgenic lines of each construct were analyzed for hypocotyl length (Appendix Fig S1), *HFR1* transcript levels and 3xHA-tagged protein abundance. In these lines, HFR1 biological activity was estimated as the difference in hypocotyl length of seedlings grown under W+FR (Hyp_{W+FR}) and W (Hyp_{W}) (Hyp_{W+FR}-Hyp_{W}) (Molina-Contreras *et al*, 2019). The potential to suppress the hypocotyl elongation in shade below that of *hfr1-5* seedlings would depend on the transcript level of *HFR1* and/or its protein levels. The *hfr1>pAt:ChHFR1* lines had shorter hypocotyls in shade (i.e., stronger global HFR1 activity) compared to *hfr1>pAt:AtHFR1* lines of similar *HFR1* expression levels (Figs 3B, C, EV3C),

suggesting that total HFR1 activity was higher in *hfr1>pAt:ChHFR1* than in *hfr1>pAt:AtHFR1* lines. However we observed much higher abundance of HFR1-3xHA protein after shade exposure in *hfr1>pAt:ChHFR1* lines than in *hfr1>pAt:AtHFR1* lines with comparable levels of *HFR1* expression (Fig 3D), suggesting that the ChHFR1 protein might be much more stable. Together, these results point to differences in protein stability (rather than in specific activity) as the main cause for the enhanced HFR1 total activity of ChHFR1 compared to AtHFR1 in complemented lines.

AtHFR1 stability is affected by light conditions. In etiolated seedlings, exposure to W promotes stabilization and accumulation of AtHFR1, whereas in W-grown seedlings, high intensity of W increases its abundance (Duek *et al*, 2004; Yang *et al*, 2005). Importantly, AtHFR1 stability has a strong impact on its biological activity as overexpression of stable forms of this protein leads to phenotypes resulting from enhanced HFR1 activity (Galstyan *et al*, 2011; Yang *et al*, 2005). As AtHFR1 and ChHFR1 primary structures are globally similar (Fig EV4A), we aimed to test if ChHFR1 stability is also light-dependent. We first examined ChHFR1 protein accumulation in response to different W intensities in seedlings of an *A. thaliana hfr1-5* line that constitutively express *ChHFR1* (*hfr1>35S:ChHFR1*) (Fig EV4B). When grown in our normal W conditions (~20 µmol m^{-2} s^{-1}), these seedlings accumulated low but detectable levels of ChHFR1; when transferred to higher W intensity (~100 µmol m^{-2} s^{-1}), ChHFR1 levels increased 10-fold (Fig EV4C). As *ChHFR1* is expressed under the constitutive 35S promoter, these results indicate that ChHFR1 protein accumulation is induced by high W intensity, as it has been described for AtHFR1 (Yang *et al*, 2005). This prompted us to pretreat W-grown seedlings

with 3 h of high W intensity in all our subsequent experiments to analyze ChHFR1 levels.

Next, we exposed *hfr1>pAt:ChHFR1* (line #22) and *hfr1>pAt:AtHFR1* (line #13) seedlings to W+FR (Fig 4A). Although *HFR1* expression in both lines was similarly induced after 3 h of W+FR, *hfr1>pAt:ChHFR1* line displayed higher levels of recombinant HFR1 protein compared to *hfr1>pAt:AtHFR1* line after 3-6 h of W+FR exposure (Fig 4A), suggesting a higher stability of the *C. hirsuta* protein compared to the *A. thaliana* orthologue. ChHFR1 protein is more abundant than AtHFR1 also when transiently expressed to comparable levels in *Nicotiana benthamiana* (tobacco) leaves (Fig 4B, C). This indicates that the higher abundance of ChHFR1 is an intrinsic property of the protein that resides in its primary structure.

AtHFR1 is known to be targeted for degradation via the 26S proteasome in dark-grown seedlings. Shade also promotes AtHFR1 degradation compared to non-shade treatments (Pacin *et al*, 2016). Hence, ChHFR1 abundance might be similarly targeted, and the increased ChHFR1 protein stability might be due to differences in degradation kinetics, likely by the 26S proteasome. We addressed this possibility by treating tobacco leaf discs overexpressing *ChHFR1* and *AtHFR1* with the protein synthesis inhibitor cycloheximide (CHX) combined with shade (Fig 4D). This treatment resulted in a decrease in ChHFR1 and AtHFR1 protein levels. However, ChHFR1 degradation was significantly slower than that of AtHFR1 (Fig 4D), supporting that changes in degradation kinetics likely contribute to the observed differences in stability between ChHFR1 and AtHFR1.

Light- and shade-regulated degradation of AtHFR1 requires binding to COP1 and the COP1 E3 ubiquitin ligase activity. Binding to COP1 results in HFR1 ubiquitination, which targets HFR1 for degradation via the 26S proteasome (Jang *et al*, 2005; Pacin *et al*, 2016; Yang *et al*, 2005). COP1-interacting proteins harbor sequence-divergent Val-Pro (VP) motifs that bind the COP1 WD40 domain with different affinities (Lau *et al*, 2019).

Inspection of the COP1 WD40 - AtHFR1 complex structure (Lau *et al*, 2019) revealed that sequence differences between AtHFR1 and ChHFR1 map to the N-terminus of the VP peptide involved in the interaction with COP1 (Fig 5A). We hypothesized that these sequence variations between HFR1 species may result in different COP1 binding affinities, affecting targeting and subsequent degradation of the two HFR1 orthologues. We thus quantified the interaction of synthetic AtHFR1 and ChHFR1 VP peptides with COP1 using microscale thermophoresis (MST, see Methods). AtHFR1 bound the COP1 WD40 domain with a dissociation constant (k_D) of ~120 µM (Fig 5B, EV5). The ChHFR1 VP peptide showed only weak binding to COP1 WD40, with a k_D in the millimolar range (Fig 5B, EV5). Importantly, a second putative VP sequence in At/ChHFR1 showed no detectable binding, while the previously characterized *A. thaliana* cryptochrome 1 (AtCRY1) and the human HsTRIB1 VP sequences bound COP1 WD40 with a k_D in the ~1 µM range, in good agreement with earlier isothermal titration calorimetry binding assays (Figs 5B, EV5) (Lau *et al*, 2019). Taken together, AtHFR1 VP peptide interacted more strongly with COP1 WD40, suggesting that AtHFR1 may represent a better substrate for COP1 than ChHFR1.

Next we aimed to explore if these differences in COP1 affinity had an impact in the subsequent degradation of AtHFR1 and ChHFR1 proteins. To test this possibility, we generated chimeric *HFR1* genes in which the VP region was swapped, named as *ChHFR1** and *AtHFR1** (Fig 5C). *ChHFR1** differed from *ChHFR1* in the VP region, that was substituted for the AtHFR1-VP1. Reciprocally, *AtHFR1** contained the ChHFR1-VP region. Like the wild-type versions, these *HFR1* derivative genes were fused to the 3xHA and placed under the control of the 35S promoter (Fig 5C). When transiently expressed in tobacco leaves, ChHFR1* was now less abundant than AtHFR1*, suggesting that the VP regions contain enough information to determine the pattern of stability of the resulting HFR1 protein (Fig 5D). Because AtHFR1-VP1 binds to COP1 WD40 domain with higher affinity than ChHFR1-VP1, these results indicate a negative correlation of the binding affinity to COP1 with the accumulation (i.e., the higher the affinity the lower the accumulation). Hence, we concluded that in the HFR1 context, a stronger binding to COP1 results in lower abundance.

HFR1 interacts with PIF7

AtHFR1 has been shown to interact with all the members of the photolabile AtPIF quartet (PIF1, PIF3, PIF4 and PIF5). Using a yeast two-hybrid (Y2H) assay, we observed that AtHFR1 homodimerized, which indicated that its HLH domain is functional in this assay (Fig 6A). In the same assay, AtHFR1 was also shown to interact with AtPIF7 (Fig 6A). These results agree with recent data (Zhang *et al*, 2019). Because AtPIF7 is the main PIF in *A. thaliana* promoting hypocotyl elongation in response to low R:FR (Li *et al*, 2012), we

aimed to address whether HFR1 also interacts genetically with PIF7. First, we analyzed the genetic interaction between AtHFR1 and AtPIF7. After crossing *A. thaliana hfr1-5* with *pif7-1* and *pif7-2* mutants, we analyzed the hypocotyl response of the obtained double mutants in different low R:FR conditions. As expected, *hfr1* hypocotyls were longer and those of *pif7* mutants were shorter compared to At^{WT} under both W+FR conditions used (Fig 6B). In W and low R:FR (0.06), double *pif7 hfr1* mutant seedlings behaved mostly as *pif7* single mutants. However, under very low R:FR (0.02), they elongated similar to At^{WT} hypocotyls (Fig 6B). Together, these results indicate that *pif7* is epistatic over *hfr1* under low R:FR, whereas it seems additive under very low R:FR, two conditions that we speculate as mimicking proximity and canopy shade, respectively (Martinez-Garcia *et al*, 2014).

To further analyze the HFR1-PIF7 interaction, we aimed to test if *HFR1* overexpression will interfere with *PIF7* overexpression and impede its effects. For HFR1, we used a line overexpressing a stable but truncated form of the protein (missing the N-terminal, 35S:GFP-ΔNt-HFR1, line #03) that strongly inhibits shade-induced hypocotyl elongation in *A. thaliana* without affecting other aspects of the seedling development (Galstyan *et al*, 2011) (Fig 6C, D). For PIF7 we used two available 35S:PIF7-CFP lines (#1 and #2) (Leivar *et al*, 2008) that were almost unresponsive to W+FR (Fig 6C) and smaller and less developed than the At^{WT} in W (Fig 6D). The inhibition of shade-induced elongation observed in the 35S:PIF7-CFP lines contrasts with the positive effect of growth observed by several other authors when overexpressing PIF7 fused to smaller tags (Flash-tag peptide) (Li *et al*, 2012), likely caused by toxic or squelching effects caused by high levels of the PIF7-CFP protein. In W,

35S:GFP-ΔNt-HFR1 35S:PIF7-CFP double transgenic seedlings (#1 and #2) did not differ in hypocotyl length and general aspect with At^{WT}; interestingly they did elongate clearly in low and very low R:FR (Fig 6C, D). The recovery of the shade-induced hypocotyl elongation and size of the seedlings took place even though *HFR1* transcript levels were significantly lower than in the 35S:GFP-ΔNt-HFR1 parental line. *PIF7* transcript levels were not significantly different in the double transgenic seedlings than in their respective parental lines (Appendix Fig S2). Therefore, the inhibitory effect of *PIF7-CFP* overexpression appeared to be counteracted by the overexpression of the truncated *HFR1*, further supporting the genetic interaction between HFR1 and PIF7 (Fig 6C, D).

Altogether, these analyses support that HFR1 and PIF7 interaction is important for the regulation of hypocotyl elongation in response to shade. These results are consistent with HFR1 functioning as a suppressor of PIF7.

HFR1 restrains PIF activity in *C. hirsuta*

The similarity between shade-induced and warm temperature-induced hypocotyl elongation (thermomorphogenesis) suggests common underlying mechanisms. In *A. thaliana*, the increased activity of HFR1 at warm temperatures was previously shown to provide an important restraint on PIF4 action that drives elongation growth (Foreman *et al*, 2011). Similarly, we hypothesized that the increased activity of HFR1 in *C. hirsuta* might restrain PIF activity more efficiently and consequently alter thermomorphogenesis (Fig 7A). We analyzed this response by growing seedlings constantly at 22ºC, 28ºC, or transferred from 22ºC to 28ºC after day 2 (Fig 7B). Whereas warm temperature promoted hypocotyl elongation of At^{WT} seedlings compared to those growing at

22ºC, *pifq* and *pif7-2* mutant seedlings were almost unresponsive to 28ºC, in accordance with the role of PIF4, PIF5 and PIF7 in thermomorphogenesis (Fiorucci *et al*, 2020; Franklin *et al*, 2011; Stavang *et al*, 2009). Unlike the *hfr1-5* mutant, which was slightly but significantly more responsive than At^{WT}, *A. thaliana* seedlings that overexpress a stable form of HFR1 (35S:GFP-ΔNt-HFR1, ΔNtHFR1) were almost unresponsive to 28ºC (Fig 7C), indicating that HFR1 activity impacts this PIF-dependent response. A lack of hypocotyl elongation was also observed in Ch^{WT} at 28ºC, a response that was recovered in the *C. hirsuta chfr1* mutant seedlings (Fig 7C). These results support our hypothesis that a strong suppression of PIFs by the enhanced HFR1 activity is responsible for the lack of hypocotyl elongation at 28ºC of Ch^{WT} seedlings (Fig 7A). Together, our results suggest that the activity of the PIF-HFR1 regulatory module might be a general mechanism to coordinate the hypocotyl elongation in response to both W+FR exposure and 28ºC.

We also studied dark-induced senescence (DIS), another PIF-dependent process (Fig 7D). In *A. thaliana*, DIS can be induced by transferring light grown seedlings to complete darkness, a process in which PIF4 and PIF5 have major roles (Liebsch & Keech, 2016; Sakuraba *et al*, 2014; Song *et al*, 2014). DIS results in a degradation of chlorophylls, which can be quantified as markers of senescence progression (Sakuraba *et al*, 2014; Song *et al*, 2014). To examine DIS, we transferred light-grown At^{WT}, *pifq* and Ch^{WT} seedlings to total darkness for up to 20 days (Fig 7E). After DIS was activated, At^{WT} seedlings became pale and eventually died. After just 5 days of darkness, chlorophyll levels dropped, and longer dark treatments resulted in pronounced differences between the three genotypes. At^{WT} seedlings became visibly yellow at day 10, accompanied

by a strong reduction of chlorophyll levels that dropped to less than 10% (Fig 7F). DIS was delayed in 35S:GFP-ΔNt-HFR1 seedlings, supporting that a stable HFR1 form can interfere with PIF activity in regulating this trait. However, DIS in was not advanced in *hfr1* mutants (Fig 7E). In Ch^{WT} seedlings, chlorophyll levels declined more slowly and seedlings were still green after 20 days of darkness, just like *pifq* (Fig 7E). The observed delay in the DIS in *C. hirsuta* was not affected in *chfr1* mutants, suggesting that HFR1 does not regulate this trait in any of the two species. It also pointed to a reduced PIF activity as the main cause for the delayed DIS in this species (Fig 7D-F). As HFR1 is very unstable, particularly in dark-grown conditions (Duek *et al*, 2004; Yang *et al*, 2005), it seems plausible that HFR1 does not accumulate in seedlings when transferred to the dark. Despite this attenuation of PIF activity, Ch^{WT} seedlings showed an etiolated phenotype similar to that of At^{WT} when grown in the dark, in contrast to *A. thaliana pifq* and 35S:GFP-ΔNt-HFR1 seedlings (Fig 7G), suggesting the PIF activity is high enough in *C. hirsuta* to induce the normal skotomorphogenic development.

DISCUSSION

It is currently unknown whether the switch between shade avoidance and tolerance strategies is an easily adjustable trait in plants. The existence of closely related species with divergent strategies to acclimate to shade provides a good opportunity to study the genetic and molecular basis for adapting to this environmental cue. To this goal, we performed comparative analyses of the hypocotyl response to shade in young seedlings of two related Brassicaceae: *A. thaliana* and *C. hirsuta*. *A. thaliana*, a model broadly used to study the SAS

hypocotyl response, is well characterized on a physiological, genetic and molecular level. *C. hirsuta* was previously described as a shade tolerant species whose hypocotyls are unresponsive to simulated shade (Hay *et al*, 2014; Molina-Contreras *et al*, 2019). Recent work showed that phyA is a major contributor to the suppression of hypocotyl elongation of *C. hirsuta* seedlings in response to shade, mainly due to the stronger phyA activity in this species compared to the shade-avoider *A. thaliana* (Molina-Contreras *et al*, 2019). Importantly, an enhanced phyA activity was not enough to explain the lack of shade-induced hypocotyl elongation in *C. hirsuta*, pointing to additional components that contribute to this response. Our aim to fill this gap led us to uncover a role for HFR1 in this response.

In *C. hirsuta*, removal of HFR1 function resulted in a strong *slender in shade* (*sis*) phenotype but milder than that of *sis1* plants, deficient in the phyA photoreceptor (Molina-Contreras *et al*, 2019), providing genetic evidence for the role of *HFR1* in restraining the *C. hirsuta* hypocotyl elongation in shade (Fig 1A, B). This indicates that, like phyA, HFR1 contributes to implement the shade tolerant habit in *C. hirsuta* seedlings. Because of the *sis* phenotype of *chfr1* and RNAi-HFR1 seedlings (Fig 1) we hypothesized that HFR1 activity is higher in *C. hirsuta* than in *A. thaliana*. Consistently, transcript levels of *HFR1* were significantly higher in Ch^{WT} than At^{WT} seedlings in both W and W+FR (Fig 2). Higher HFR1 levels in *C. hirsuta* may not be relevant in W because of the expected lower abundance and activity of PIFs, but a higher pool of ChHFR1 ready to suppress early ChPIF action in shade could provide a fast and sustained repression of the elongation response. Indeed, the shade-induced expression of *PIL1*, *YUC8* and *XTR7*, known to be direct PIF target genes in *A.*

thaliana, was strongly and rapidly enhanced in *chfr1* and RNAi-HFR1 seedlings (Fig 1C, D). More importantly, rapid shade-induced expression was globally attenuated in Ch^{WT} compared to At^{WT} seedlings (Molina-Contreras *et al*, 2019).

In addition to changes in gene expression, a higher HFR1 activity in *C. hirsuta* could also result from post-translational regulation affecting protein stability. Our immunoblot analyses indicated that HFR1 proteins rapidly accumulate in response to simulated shade (W+FR), likely as a consequence of the strong shade-induced responsiveness of the promoter (Fig 4A). These results support that regulation of HFR1 protein abundance in low R:FR occurs mainly at the transcriptional level, as suggested (de Wit *et al*, 2016). More importantly, ChHFR1 accumulates significantly more when expressed under the control of a constitutive promoter either under W or W+FR (Fig 4B-D) suggesting that intrinsic differences in post-translational stability between these proteins play a role in their contrasting accumulation.

AtHFR1 protein abundance is modified post-translationally by phosphorylation (Park *et al*, 2008) and ubiquitination in a light- and COP1-dependent manner (Jang *et al*, 2005; Yang *et al*, 2005). Canopy shade promotes nuclear accumulation of COP1 (Pacin *et al*, 2013; Pacin *et al*, 2016) allowing it to directly interact with and polyubiquitinate AtHFR1, leading to its degradation by the 26S proteasome (Huang *et al*, 2014; Jang *et al*, 2005; Yang *et al*, 2005). AtHFR1, like ChHFR1, contains two putative COP1 binding sites (VP motifs) on its N-terminal half (Fig EV4A), although only one binds COP1 (Figs 5A, EV5) (Lau *et al*, 2019). Deletion of AtHFR1 Nt leads to its stabilization in the dark and light (Duek *et al*, 2004), and results in a stronger biological activity (Galstyan *et al*, 2011; Jang *et al*, 2005; Yang *et al*, 2005), highlighting

the importance of the COP1-interacting domain for light regulation of AtHFR1 stability. Our MST binding assays showed that AtHFR1 binds to COP1 about 100 times more weakly than other plant COP1 substrates do (Lau *et al*, 2019), and ChHFR1 even more weakly than AtHFR1 (Fig 5A, B). AtHFR1 and ChHFR1 primary structures are similar, including the putative COP1-interacting domain (Jang *et al*, 2005), except for the addition of 30 amino acids at the N-terminal part of ChHFR1 and a 9-amino acid insertion in the C-terminal part of AtHFR1 (Fig EV4A). We cannot discount the possibility that protein sequence and/or structural differences other than the VP motifs could also contribute to the affinity of the full-length HFR1 orthologues for COP1 and account for the difference in abundance between *C. hirsuta* and *A. thaliana* HFR1. However, the strong impact of swapping the VP region between ChHFR1 and AtHFR1 on the abundance of the resulting HFR1* proteins (Fig 5C, D) further points to the binding affinity of COP1 for its substrates as a main determinant of the stability of the two HFR1 orthologues. Together, our results point to (1) the regulation of affinity for COP1 as impacting HFR1 stability; and (2) HFR1 stability as a mechanism to control global HFR1 activity to modulate adaptation of different plant species to vegetation proximity and shade.

AtHFR1 was previously shown to interact with all the AtPIFQ members and to form non-DNA-binding heterodimers (Fairchild *et al*, 2000; Hornitschek *et al*, 2012; Shi *et al*, 2013). Our genetic and Y2H experiments extended the list of AtHFR1 interactors to AtPIF7, the major SAS-promoting PIF (Fig 6). If ChHFR1 maintains similar PIF-binding abilities, the reduced expression of *ChPIF7* (Fig 2) might further contribute to imbalance the PIF-HFR1 module in favor of the negative HFR1 activity in *C. hirsuta* compared to *A. thaliana*. Because of the

higher stability of ChHFR1 over AtHFR1 in shade (Fig 4), an even stronger repression of global PIF activity in *C. hirsuta* would contribute to the unresponsiveness of hypocotyls to shade. The attenuation of the warm temperature-induced hypocotyl elongation in *C. hirsuta*, which is a PIF-regulated process in *A. thaliana* (Fiorucci *et al*, 2020; Hayes *et al*, 2017; Koini *et al*, 2009; Stavang *et al*, 2009) and HFR1-dependent in both species (Figs 7A-C), further agrees with our proposal of an enhanced activity of HFR1 in *C. hirsuta* compared to *A. thaliana*. On the other hand, the delayed DIS observed in *C. hirsuta*, shown to be PIF-regulated in *A. thaliana* (Sakuraba *et al*, 2014; Song *et al*, 2014) but unaffected by HFR1 in the two species analyzed (Figs 7D, E), suggests that PIF activity is globally lower *per se* in *C. hirsuta* than in *A. thaliana*. Together, our results indicate that PIF-HFR1 module is balanced differently in *C. hirsuta* by the combination of (1) an attenuated global PIF activity and *PIF7* expression compared to *A. thaliana*, and (2) the increased levels of ChHFR1 in light and shade conditions, resulting in the repression of PIF-regulated processes in *C. hirsuta* (Fig 8). Importantly, although attenuated, PIF activity in *C. hirsuta* is enough to provide a functional and effective etiolation response (Fig 7G) for seedlings survival during germination in the dark.

Activity of HFR1 and phyA (Molina-Contreras *et al*, 2019) appears to be increased in *C. hirsuta* to maintain unresponsiveness of hypocotyls to shade. An aspect shared by both negative regulators is that their expression and/or stability are strongly affected by light conditions. Expression of both *PHYA* and *HFR1* is induced by simulated shade in de-etiolated seedlings. By contrast, whereas the stability of the photolabile phyA is reduced by light but enhanced by shade, that of AtHFR1 is promoted by light and decreased by shade (Casal

et al, 2014; Ciolfi *et al*, 2013; Duek *et al*, 2004; Kircher *et al*, 1999; Martinez-Garcia *et al*, 2014; Pacin *et al*, 2016; Park *et al*, 2008; Yang *et al*, 2018). Although expression of both *PHYA* and *HFR1* is higher in *C. hirsuta* than in *A. thaliana*, different mechanisms might contribute to their increased activity in *C. hirsuta*. Indeed, enhanced ChphyA repression was achieved by its stronger specific intrinsic activity (Molina-Contreras *et al*, 2019). By contrast, enhanced ChHFR1 repression was accomplished through its higher gene expression and protein stability coupled with an attenuated PIF7 activity. Altogether this could provide a more repressive state of the *C. hirsuta* PIF-HFR1 module. Because of the temporal differences downregulating many of the shade marker genes between phyA (observed after 4-8 hours of shade exposure) (Molina-Contreras *et al*, 2019) and HFR1 (rapidly detected after just 1 h of shade exposure) (Fig 1C, D), it seems likely that ChHFR1 and ChphyA suppressor mechanisms of shade response in *C. hirsuta* act independently, as it was reported for *A. thaliana* (Ciolfi *et al*, 2013; Ortiz-Alcaide *et al*, 2019). Therefore, the concerted activity of these two independent suppressor mechanisms seems to coordinately prevent the shade-induced hypocotyl elongation in *C. hirsuta*. Whether other shade tolerant species employ the same adaptive principles is something we aim to explore in the future.

MATERIALS AND METHODS

Plant material and growth conditions

Arabidopsis thaliana hfr1-5, *pif7-1*, *pif7-2* and *pifq* mutants, 35S:PIF7-CFP and 35S:GFP-ΔNt-HFR1 lines (in the Col-0 background, At^{WT}) and *Cardamine hirsuta* (Oxford ecotype, Ox, Ch^{WT}) plants have been described

before (Galstyan *et al*, 2011; Hay *et al*, 2014; Leivar *et al*, 2008; Yang *et al*, 2005). Plants were grown in the greenhouse under long-day photoperiods (16 h light and 8 h dark) to produce seeds, as described (Gallemi *et al*, 2016; Gallemi *et al*, 2017; Martinez-Garcia *et al*, 2014). For transient expression assays, *Nicotiana benthamiana* plants were grown in the greenhouse under long-day photoperiods (16 h light and 8 h dark).

For hypocotyl assays, seeds were surface-sterilized and sown on solid growth medium without sucrose (0.5xGM–). For gene expression analyses, immunoblot experiments and pigment quantification, seeds were sown on a sterilized nylon membrane placed on top of the solid 0.5xGM– medium. After stratification (dark at 4ºC) of 3-6 days, plates with seeds were incubated in plant chambers at 22ºC under continuous white light (W) for at least 2 h to break dormancy and synchronize germination (Paulisic *et al*, 2017; Roig-Villanova *et al*, 2019).

W was emitted from cool fluorescent tubes that provided from 20 to 100 µmol m^{-2} s^{-1} of photosynthetically active radiation (PAR) with a red (R) to far-red light (FR) ratio (R:FR) from 1.3-3.3. The different simulated shade treatments were produced by supplementing W with increasing amounts of FR (W+FR). FR was emitted from GreenPower LED module HF far-red (Philips), providing R:FR of 0.02-0.09. Light fluence rates were measured with a Spectrosense2 meter (Skye Instruments Ltd), which measures PAR (400-700 nm), and 10 nm windows of R (664-674 nm) and FR (725-735 nm) regions (Martinez-Garcia *et al*, 2014). Details of the resulting light spectra have been described before (Molina-Contreras *et al*, 2019).

Temperature induced hypocotyl elongation assays were done by placing the plates with seeds under the indicated light conditions in growth chambers at 22ºC or 28ºC.

Measurement of hypocotyl length

Hypocotyl length was measured as described (Paulisic *et al*, 2017; Roig-Villanova *et al*, 2019). Experiments were repeated at least three times with more than 10 seedlings per genotype and/or treatment, providing consistent results. Hypocotyl measurements from the different experiments were averaged.

Generation of transgenic lines, mutants and crosses

A. thaliana hfr1-5 plants were transformed to express *AtHFR1* and *ChHFR1* under the promoters of 35S or *AtHFR1* (pAt). The obtained lines were named as *hfr1>35S:ChHFR1*, *hfr1>pAt:AtHFR1* and *hfr1>pAt:ChHFR1*. Transgenic RNAi-HFR1 and mutant *chfr1-1* and *chfr1-2* lines are in Ch^{WT} background. Details of the constructs used for the generation of these lines (Morineau *et al*, 2017) are provided as Appendix Supplementary Methods.

Gene expression analyses

Real-time qPCR analyses were performed using biological triplicates, as indicated (Gallemi *et al*, 2017). Total RNA was extracted from seedlings, treated as indicated, using commercial kits (Maxwell® SimplyRNA and Maxwell® RSC Plant RNA Kits; www.promega.com). 2 µg of RNA was reverse-transcribed with Transcriptor First Strand cDNA synthesis Kit (Roche, www.roche.com). The *A.*

thaliana UBIQUITIN 10 (*UBQ10*) was used for normalization in *A. thaliana hfr1-5* lines expressing *AtHFR1* or *ChHFR1*. The *ELONGATION FACTOR 1α* (*EF1α*), *YELLOW-LEAF-SPECIFIC GENE 8* (*YLS8*) and *SPC25* (AT2G39960) were used for normalizing and comparing the levels of *HFR1* and *PIF7* between *A*. *thaliana* and *C. hirsuta* (Molina-Contreras *et al*, 2019). Primers sequences for qPCR analyses are provided in Appendix Table S1.

Expression of *HFR1* derivatives in *Nicotiana benthamiana*

N. benthamiana plants were agroinfiltrated with *A. tumefaciens* strains transformed with the plasmids to express the various *HFR1* derivatives, and kept in the greenhouse under long-day photoperiods. Samples (leaf circles obtained from infiltrated areas) were taken 3 days after agroinfiltration and frozen immediately. In Fig 4D, prior freezing, leaf circles were incubated in Petri dishes with 10 mL of the ±CHX solution for the indicated times and conditions. Each biological sample contained about 75 mg of leaf tissue from the same leaf. Additional details of the preparation of the plasmids used are provided in Appendix Supplementary Methods.

Protein extraction and immunoblotting analyses

To detect and quantify transgenic AtHFR1 and ChHFR1, proteins were extracted from ~50 mg of 7-day old seedlings (grown as indicated) or from 50-75 mg of agroinfiltrated *N. benthamiana* leaves. Plant material was frozen in liquid nitrogen, ground to powder and total proteins were extracted using an SDS-containing extraction buffer (1.5 µL per mg of fresh weight), as described (Gallemi *et al*, 2017). Protein concentration was estimated using Pierce™ BCA

Protein Assay Kit (Thermo Scientific, www.thermofisher.com). Proteins (45 - 50 µg per lane) were resolved on a 10% SDS-PAGE gel, transferred to a PVDF membrane and immunoblotted with rat monoclonal anti-HA (High Affinity, clone 3F10, Roche; 1:2000 dilution) or mouse monoclonal anti-GFP (monoclonal mix, clones 7.1 + 13.1, Roche; 1:2000 dilution). Secondary antibodies used were horseradish peroxidase (HRP) conjugated goat anti-rat (Polyclonal, A9037, Sigma, www.sigmaaldrich.com; 1:5000 dilution) and HRP conjugated sheep anti-mouse (Promega; 1:10000 dilution). Development of blots was carried out in ChemiDoc™ Touch Imaging System (Bio-Rad, www.bio-rad.com) using ECL Prime Western Blotting Detection Reagent (GE Healthcare, RPN2236). Relative protein levels of three to four biological replicates were quantified using Image Lab™ Software (Bio-Rad, www.bio-rad.com).

Yeast 2 Hybrid (Y2H) assays

For Y2H assays we employed a cell mating system, as described (Gallemi *et al*, 2017). The leucine (Leu) auxotroph YM4271a yeast strain was transformed with the AD-derived constructs and the tryptophan (Trp) auxotroph pJ694α strain with the BD-derived constructs. Colonies were selected on synthetic defined medium (SD) lacking Leu (SD-L) or Trp (SD-W), grown in liquid medium and set to mate by mixing equal volumes of transformed cells. Dilutions of the mated cells were selected on SD-LW and protein interactions were tested on SD-LW medium lacking histidine (SD-HLW). Details of the yeast constructs used are provided as Appendix Supplementary Methods.

Expression of AtCOP1 WD40 protein and purification

AtCOP1 WD40 (residues 349-675) was expressed in *Spodoptera frugiperda* Sf9 cells (Thermofisher) and purified as described previously (Lau *et al*, 2019). Details of the procedure are provided as Appendix Supplementary Methods.

Protein labeling and Microscale thermophoresis (MST)

COP1 WD40 was labeled using Monolith Protein Labeling Kit RED-NHS 2nd Generation Amine Reactive kit (MO-L011, Nanotemper Technologies, Munich, Germany). After the TEV cleavage, COP1 WD40 was in buffer A containing 2 mM β-ME, which is incompatible with the labeling procedure. Therefore, prior to labeling, the buffer was exchanged using labeling buffer NHS provided in the kit. In the last step, the protein was purified from the free dye, in the assay buffer 20 mM Hepes pH 7.5, 150 mM NaCl, 2 mM TCEP and 0.05% [v/v] Tween-20 in 12 to 15 different fractions. The absorbance of each sample was measured at 280 nm and 650 nm. The Degree of Labeling (DOL) was calculated using the formula provided in the manual. Aliquots containing 2000 to 8000 nM concentration of proteins and DOL of >0.5 were flash frozen for the use in the assay.

Peptide solutions were freshly prepared in the assay buffer at desired concentrations. For each independent replicate, 10 µL of peptide solution was serially diluted 1:1 using assay buffer, in 16 PCR tubes. 10 µL of solution was discarded from the 16th tube, thus each tube contained 10 µL of peptide solution. Each dilution step was mixed with 10 µL of 150 nM of COP1 WD40 and transferred into Monolith NT.115 Premium Capillaries (MO-K025). The samples were measured with the Monolith NT.115 instrument at a 25% LED

Power and 20% MST power. The resulting thermophoresis data were analyzed with the MOAffinityAnalysis software (Nanotemper Technologies).

DATA AVAILABILITY

This study includes no data deposited in external repositories.

ACKNOWLEDGEMENTS

We are grateful to Peter Quail (PGEC, Albany, CA, USA) for providing 35S:PIF7-CFP seeds; and to Manuel Rodriguez-Concepción (CRAG) for comments on the manuscript. SP received predoctoral fellowships from the *Agència d'Ajuts Universitaris i de Recerca* (AGAUR - Generalitat de Catalunya, FI program). WQ is a recipient of a predoctoral Chinese Scholarship Council (CSC) fellowship. CT received a Marie Curie IEF postdoctoral contract funded by the European Commission and a CRAG short-term fellowship. We also acknowledge the support of the MINECO for the "Centro de Excelencia Severo Ochoa 2016-2019" award SEV-2015-0533 and by the CERCA Programme / Generalitat de Catalunya. FN research at the IJPB benefits from the support of the LabEx Saclay Plant Sciences-SPS (ANR-10-LABX-0040-SPS). Our research is supported by grants from BBSRC (BB/H006974/1) and Max Planck Society (core grant) to MT, and from MINECO-FEDER (BIO2017-85316-R) and AGAUR (2017-SGR1211 and Xarba) to JFM-G. MH is an International Research Scholar by the Howard Hughes Medical Institute.

AUTHOR CONTRIBUTIONS

JFM-G conceived the original research plan, and directed and coordinated the study. SP, WQ, CT, BA and FN designed and/or carried out experiments using *A. thaliana* and *C. hirsuta*. MT and FN fundamentally contributed to design the constructs to obtain *C. hirsuta* transgenic and mutant lines. HA-V and MH designed and performed MST experiments and their analyses. SP and JFM-G wrote the article with contributions and/or comments of all other authors.

CONFLICT OF INTEREST

The authors declare that they have no conflict of interest.

REFERENCES

Ballare CL, Pierik R (2017) The shade-avoidance syndrome: multiple signals and ecological consequences. *Plant Cell Environ* **40:** 2530-2543

Bou-Torrent J, Galstyan A, Gallemi M, Cifuentes-Esquivel N, Molina-Contreras MJ, Salla-Martret M, Jikumaru Y, Yamaguchi S, Kamiya Y, Martinez-Garcia JF (2014) Plant proximity perception dynamically modulates hormone levels and sensitivity in Arabidopsis. *J Exp Bot* **65:** 2937-2947

Casal JJ (2013) Photoreceptor signaling networks in plant responses to shade. *Annu Rev Plant Biol* **64:** 403-427

Casal JJ, Candia AN, Sellaro R (2014) Light perception and signalling by phytochrome A. *J Exp Bot* **65:** 2835-2845

Cifuentes-Esquivel N, Bou-Torrent J, Galstyan A, Gallemi M, Sessa G, Salla Martret M, Roig-Villanova I, Ruberti I, Martinez-Garcia JF (2013) The bHLH proteins BEE and BIM positively modulate the shade avoidance syndrome in Arabidopsis seedlings. *The Plant Journal* **75:** 989-1002

Ciolfi A, Sessa G, Sassi M, Possenti M, Salvucci S, Carabelli M, Morelli G, Ruberti I (2013) Dynamics of the shade-avoidance response in Arabidopsis. *Plant Physiol* **163:** 331-353

de Wit M, Keuskamp DH, Bongers FJ, Hornitschek P, Gommers CMM, Reinen E, Martinez-Ceron C, Fankhauser C, Pierik R (2016) Integration of Phytochrome and Cryptochrome Signals Determines Plant Growth during Competition for Light. *Curr Biol* **26:** 3320-3326

Duek PD, Elmer MV, van Oosten VR, Fankhauser C (2004) The degradation of HFR1, a putative bHLH class transcription factor involved in light signaling, is regulated by phosphorylation and requires COP1. *Curr Biol* **14:** 2296-2301

Fairchild CD, Schumaker MA, Quail PH (2000) HFR1 encodes an atypical bHLH protein that acts in phytochrome A signal transduction. *Genes Dev* **14:** 2377-2391

Fiorucci AS, Fankhauser C (2017) Plant Strategies for Enhancing Access to Sunlight. *Curr Biol* **27:** R931-R940

Fiorucci AS, Galvao VC, Ince YC, Boccaccini A, Goyal A, Allenbach Petrolati L, Trevisan M, Fankhauser C (2020) PHYTOCHROME INTERACTING FACTOR 7 is important for early responses to elevated temperature in Arabidopsis seedlings. *New Phytol* **226:** 50-58

Foreman J, Johansson H, Hornitschek P, Josse EM, Fankhauser C, Halliday KJ (2011) Light receptor action is critical for maintaining plant biomass at warm ambient temperatures. *Plant J* **65:** 441-452

Franklin KA, Lee SH, Patel D, Kumar SV, Spartz AK, Gu C, Ye S, Yu P, Breen G, Cohen JD *et al* (2011) Phytochrome-interacting factor 4 (PIF4)

regulates auxin biosynthesis at high temperature. *Proc Natl Acad Sci U S A* **108:** 20231-20235

Galstyan A, Cifuentes-Esquivel N, Bou-Torrent J, Martinez-Garcia JF (2011) The shade avoidance syndrome in Arabidopsis: a fundamental role for atypical basic helix-loop-helix proteins as transcriptional cofactors. *Plant J* **66:** 258-267

Gallemi M, Galstyan A, Paulisic S, Then C, Ferrandez-Ayela A, Lorenzo-Orts L, Roig-Villanova I, Wang X, Micol JL, Ponce MR *et al* (2016) DRACULA2 is a dynamic nucleoporin with a role in regulating the shade avoidance syndrome in Arabidopsis. *Development* **143:** 1623-1631

Gallemi M, Molina-Contreras MJ, Paulisic S, Salla-Martret M, Sorin C, Godoy M, Franco-Zorrilla JM, Solano R, Martinez-Garcia JF (2017) A non-DNA-binding activity for the ATHB4 transcription factor in the control of vegetation proximity. *New Phytol* **216:** 798-813

Gommers CM, Keuskamp DH, Buti S, van Veen H, Koevoets IT, Reinen E, Voesenek LA, Pierik R (2017) Molecular Profiles of Contrasting Shade Response Strategies in Wild Plants: Differential Control of Immunity and Shoot Elongation. *Plant Cell* **29:** 331-344

Gommers CM, Visser EJ, St Onge KR, Voesenek LA, Pierik R (2013) Shade tolerance: when growing tall is not an option. *Trends Plant Sci* **18:** 65-71

Hay AS, Pieper B, Cooke E, Mandakova T, Cartolano M, Tattersall AD, Ioio RD, McGowan SJ, Barkoulas M, Galinha C *et al* (2014) Cardamine hirsuta: a versatile genetic system for comparative studies. *Plant J* **78:** 1-15

Hayes S, Sharma A, Fraser DP, Trevisan M, Cragg-Barber CK, Tavridou E, Fankhauser C, Jenkins GI, Franklin KA (2017) UV-B Perceived by the

UVR8 Photoreceptor Inhibits Plant Thermomorphogenesis. *Curr Biol* **27:** 120-127

Hersch M, Lorrain S, de Wit M, Trevisan M, Ljung K, Bergmann S, Fankhauser C (2014) Light intensity modulates the regulatory network of the shade avoidance response in Arabidopsis. *Proc Natl Acad Sci U S A* **111:** 6515-6520

Hornitschek P, Kohnen MV, Lorrain S, Rougemont J, Ljung K, Lopez-Vidriero I, Franco-Zorrilla JM, Solano R, Trevisan M, Pradervand S *et al* (2012) Phytochrome interacting factors 4 and 5 control seedling growth in changing light conditions by directly controlling auxin signaling. *Plant J* **71:** 699-711

Hornitschek P, Lorrain S, Zoete V, Michielin O, Fankhauser C (2009) Inhibition of the shade avoidance response by formation of non-DNA binding bHLH heterodimers. *EMBO J* **28:** 3893-3902

Huang X, Ouyang X, Deng XW (2014) Beyond repression of photomorphogenesis: role switching of COP/DET/FUS in light signaling. *Curr Opin Plant Biol* **21:** 96-103

Jang IC, Yang JY, Seo HS, Chua NH (2005) HFR1 is targeted by COP1 E3 ligase for post-translational proteolysis during phytochrome A signaling. *Genes Dev* **19:** 593-602

Kircher S, Kozma-Bognar L, Kim L, Adam E, Harter K, Schafer E, Nagy F (1999) Light quality-dependent nuclear import of the plant photoreceptors phytochrome A and B. *Plant Cell* **11:** 1445-1456

Koini MA, Alvey L, Allen T, Tilley CA, Harberd NP, Whitelam GC, Franklin KA (2009) High temperature-mediated adaptations in plant architecture require the bHLH transcription factor PIF4. *Curr Biol* **19:** 408-413

Lau K, Podolec R, Chappuis R, Ulm R, Hothorn M (2019) Plant photoreceptors and their signaling components compete for COP1 binding via VP peptide motifs. *EMBO J***:** e102140

Leivar P, Monte E, Al-Sady B, Carle C, Storer A, Alonso JM, Ecker JR, Quail PH (2008) The Arabidopsis phytochrome-interacting factor PIF7, together with PIF3 and PIF4, regulates responses to prolonged red light by modulating phyB levels. *Plant Cell* **20:** 337-352

Li L, Ljung K, Breton G, Schmitz RJ, Pruneda-Paz J, Cowing-Zitron C, Cole BJ, Ivans LJ, Pedmale UV, Jung HS *et al* (2012) Linking photoreceptor excitation to changes in plant architecture. *Genes Dev* **26:** 785-790

Liebsch D, Keech O (2016) Dark-induced leaf senescence: new insights into a complex light-dependent regulatory pathway. *New Phytol* **212:** 563-570

Lorrain S, Allen T, Duek PD, Whitelam GC, Fankhauser C (2008) Phytochrome-mediated inhibition of shade avoidance involves degradation of growth-promoting bHLH transcription factors. *Plant J* **53:** 312-323

Martinez-Garcia JF, Gallemi M, Molina-Contreras MJ, Llorente B, Bevilaqua MR, Quail PH (2014) The shade avoidance syndrome in Arabidopsis: the antagonistic role of phytochrome a and B differentiates vegetation proximity and canopy shade. *PLoS One* **9:** e109275

Martinez-Garcia JF, Huq E, Quail PH (2000) Direct targeting of light signals to a promoter element-bound transcription factor. *Science* **288:** 859-863

Mazza CA, Ballare CL (2015) Photoreceptors UVR8 and phytochrome B cooperate to optimize plant growth and defense in patchy canopies. *New Phytol* **207:** 4-9

Molina-Contreras MJ, Paulisic S, Then C, Moreno-Romero J, Pastor-Andreu P, Morelli L, Roig-Villanova I, Jenkins H, Hallab A, Gan X *et al* (2019) Photoreceptor Activity Contributes to Contrasting Responses to Shade in Cardamine and Arabidopsis Seedlings. *Plant Cell* **31:** 2649-2663

Morineau C, Bellec Y, Tellier F, Gissot L, Kelemen Z, Nogue F, Faure JD (2017) Selective gene dosage by CRISPR-Cas9 genome editing in hexaploid Camelina sativa. *Plant Biotechnol J* **15:** 729-739

Ortiz-Alcaide M, Llamas E, Gomez-Cadenas A, Nagatani A, Martinez-Garcia JF, Rodriguez-Concepcion M (2019) Chloroplasts Modulate Elongation Responses to Canopy Shade by Retrograde Pathways Involving HY5 and Abscisic Acid. *Plant Cell* **31:** 384-398

Pacin M, Legris M, Casal JJ (2013) COP1 re-accumulates in the nucleus under shade. *Plant J* **75:** 631-641

Pacin M, Semmoloni M, Legris M, Finlayson SA, Casal JJ (2016) Convergence of CONSTITUTIVE PHOTOMORPHOGENESIS 1 and PHYTOCHROME INTERACTING FACTOR signalling during shade avoidance. *New Phytol* **211:** 967-979

Park HJ, Ding L, Dai M, Lin R, Wang H (2008) Multisite phosphorylation of Arabidopsis HFR1 by casein kinase II and a plausible role in regulating its degradation rate. *J Biol Chem* **283:** 23264-23273

Paulisic S, Molina-Contreras MJ, Roig-Villanova I, Martinez-Garcia JF (2017) Approaches to Study Light Effects on Brassinosteroid Sensitivity. *Methods Mol Biol* **1564:** 39-47

Pierik R, Testerink C (2014) The art of being flexible: how to escape from shade, salt, and drought. *Plant Physiol* **166:** 5-22

Roig-Villanova I, Bou-Torrent J, Galstyan A, Carretero-Paulet L, Portoles S, Rodriguez-Concepcion M, Martinez-Garcia JF (2007) Interaction of shade avoidance and auxin responses: a role for two novel atypical bHLH proteins. *The EMBO Journal* **26:** 4756-4767

Roig-Villanova I, Paulisic S, Martinez-Garcia JF (2019) Shade Avoidance and Neighbor Detection. *Methods Mol Biol* **2026:** 157-168

Sakuraba Y, Jeong J, Kang MY, Kim J, Paek NC, Choi G (2014) Phytochrome-interacting transcription factors PIF4 and PIF5 induce leaf senescence in Arabidopsis. *Nat Commun* **5:** 4636

Sasidharan R, Pierik R (2010) Cell wall modification involving XTHs controls phytochrome-mediated petiole elongation in Arabidopsis thaliana. *Plant Signal Behav* **5:** 1491-1492

Sessa G, Carabelli M, Sassi M, Ciolfi A, Possenti M, Mittempergher F, Becker J, Morelli G, Ruberti I (2005) A dynamic balance between gene activation and repression regulates the shade avoidance response in Arabidopsis. *Genes Dev* **19:** 2811-2815

Shi H, Zhong S, Mo X, Liu N, Nezames CD, Deng XW (2013) HFR1 sequesters PIF1 to govern the transcriptional network underlying light-initiated seed germination in Arabidopsis. *Plant Cell* **25:** 3770-3784

Smith H (1982) Light quality, photoperception, and plant strategy. *Ann Rev Plant Physiol* **33:** 481-518

Song Y, Yang C, Gao S, Zhang W, Li L, Kuai B (2014) Age-triggered and dark-induced leaf senescence require the bHLH transcription factors PIF3, 4, and 5. *Mol Plant* **7:** 1776-1787

Stavang JA, Gallego-Bartolome J, Gomez MD, Yoshida S, Asami T, Olsen JE, Garcia-Martinez JL, Alabadi D, Blazquez MA (2009) Hormonal regulation of temperature-induced growth in Arabidopsis. *Plant J* **60:** 589-601

Valladares F, Niinemets U (2008) Shade Tolerance, a Key Plant Feature of Complex Nature and Consequences. *Ann Rev Ecol, Evol Syst* **39:** 237-257

van Gelderen K, Kang C, Paalman R, Keuskamp D, Hayes S, Pierik R (2018) Far-Red Light Detection in the Shoot Regulates Lateral Root Development through the HY5 Transcription Factor. *Plant Cell* **30:** 101-116

Yang C, Li L (2017) Hormonal Regulation in Shade Avoidance. *Front Plant Sci* **8:** 1527

Yang C, Xie F, Jiang Y, Li Z, Huang X, Li L (2018) Phytochrome A Negatively Regulates the Shade Avoidance Response by Increasing Auxin/Indole Acidic Acid Protein Stability. *Dev Cell* **44:** 29-41 e24

Yang J, Lin R, Sullivan J, Hoecker U, Liu B, Xu L, Deng XW, Wang H (2005) Light regulates COP1-mediated degradation of HFR1, a transcription factor essential for light signaling in Arabidopsis. *Plant Cell* **17:** 804-821

Zhang R, Yang C, Jiang Y, Li L (2019) A PIF7-CONSTANS-Centered Molecular Regulatory Network Underlying Shade-Accelerated Flowering. *Mol Plant* **12:** 1587-1597

FIGURE LEGENDS

Figure 1. Hypocotyls of *C. hirsuta* seedlings with reduced levels of *ChHFR1* strongly elongate in response to simulated shade.

A, **B** Hypocotyl length of Ch^{WT}, **(A)** RNAi-ChHFR1 transgenic and **(B)** *chfr1* mutant seedlings grown under different R:FR. Seedlings were grown for 7 days in continuous W (R:FR>1.5) or for 3 days in W then transferred to W supplemented with increasing amounts of FR (W+FR) for 4 more days, producing various R:FR. Aspect of representative 7-day old Ch^{WT}, RNAi-HFR1 and *chfr1-1* seedlings grown in W or W+FR (R:FR, 0.02), as indicated, is shown in lower panel.

C, **D** Effect of W+FR exposure on the expression of *PIL1*, *YUC8* and *XTR7* genes in seedlings of Ch^{WT}, **(C)** RNAi-HFR1 and **(D)** c*hfr1* mutant lines. Expression was analyzed in 7-day old W-grown seedlings transferred to W+FR (R:FR, 0.02) for 0, 1, 4, 8 and 12 h. Transcript abundance is normalized to *EF1α* levels.

Data information: Values are the means ± SE of three independent biological replicates relative to Ch^{WT} value at 0 h. Asterisks mark significant differences (Student *t*-test: ** p-value <0.01; * p-value <0.05) relative to Ch^{WT} value at the same time point.

Figure 2. Levels of *HFR1* transcript are higher in *C. hirsuta* than *A. thaliana* seedlings.

Seedlings of Ch^{WT} and At^{WT} were grown for 3 days in W then either kept under the same conditions or transferred to W+FR (R:FR, 0.02) for the indicated times. Plant material was harvested every 24 h. Transcript abundance of *HFR1* and *PIF7* was normalized to three reference genes (*EF1α*, *SPC25*, and *YLS8*). Expression values are the means ± SE of three independent biological replicates relative to the data of At^{WT} grown in continuous W at day 3. Asterisks mark significant differences (2-way ANOVA: ** p-value <0.01, *** p-value <0.001) between Ch^{WT} and At^{WT} when grown under W (black asterisks) or W+FR (red asterisks).

Figure 3. The activity of ChHFR1 is higher than that of AtHFR1 in *A. thaliana* seedlings.

A Cartoon of constructs containing *ChHFR1* or *AtHFR1* under the *HFR1* promoter of *A. thaliana* (*pAtHFR1*) used to complement *hfr1-5* mutant of *A. thaliana* (At *hfr1-5*).

B Relative expression of *HFR1* in seedlings of At^{WT}, At *hfr1*-5, hfr1>*pAt:ChHFR1* (in blue) and *hfr1>pAt:AtHFR1* (in red) lines grown under W+FR (R:FR, 0.02). Expression values are the means ± SE of three independent biological replicates relative to the data of 7 days old At^{WT}. Transcript abundance is normalized to *UBQ10* levels.

C Elongation response of seedlings of the indicated lines grown for 7 days in continuous W or 2 days in W then transferred for 5 days to W+FR (R:FR, 0.02). The mean hypocotyl length in W (Hyp_W) and W+FR (Hyp_{W+FR}) of at least four

biological replicates was used to calculate Hyp_{W+FR}-Hyp_{W}. Error bars represent SE.

D Relative HFR1 protein levels in seedlings of the indicated lines, normalized to actin protein levels, are the means ± SE of three independent biological replicates relative to *hfr1>pAt:ChHFR1* line #22 that is taken as 1. Seedlings were grown for 7 days in continuous W (~20 µmol m^{-2} s^{-1}) after which they were incubated for 3 h in high W (~100 µmol m^{-2} s^{-1}) and transferred to W+FR (R:FR, 0.06) for 3 h.

Data information: Different letters denote significant differences (one-way ANOVA with Tukey test, p-value <0.05) among means.

Figure 4. ChHFR1 and AtHFR1 proteins show different stability in shade.

A Expression of *HFR1* and protein levels of HFR1-3xHA in seedlings of *hfr1>pAt:ChHFR1* (line #22) and *hfr1>pAt:AtHFR1* (line #13). Seedlings were grown for 7 days in continuous W (~20 µmol m^{-2} s^{-1}) after which they were incubated for 3 h in high W (~100 µmol m^{-2} s^{-1}) and then either kept at high W or transferred to W+FR (R:FR, 0.06) for 3 or 6 h, as indicated in the cartoon at the top. Relative *HFR1* transcript levels, normalized to *UBQ10*, are the means ± SE of three independent biological replicates relative to *hfr1>pAt:ChHFR1* #22 grown for 3 h under W+FR. Relative protein levels, normalized to actin, are the means ± SE of three independent biological replicates relative to *hfr1>pAt:ChHFR1* #22. Samples were collected at data points marked in the cartoon with asterisks.

B Cartoon of constructs containing *ChHFR1* or *AtHFR1* under the *35S* promoter used for transient expression of transgenes in *N. benthamiana* leaves.

C Relative *HFR1* transcript levels transiently expressed in tobacco leaves, normalized to the *GFP*, are the means ± SE of three independent biological replicates (left). Relative HFR1 protein levels, normalized to the GFP levels, are the means ± SE of four independent biological replicates (right). In **A** and **C**, asterisks mark significant differences (Student *t*-test: * p-value <0.05, ** p-value <0.01) between the indicated pairs.

D Degradation of ChHFR1 (*35S:ChHFR1*) and AtHFR1 (*35S:AtHFR1*) in tobacco leaf discs treated with cycloheximide (CHX, 100 µM) for the indicated times. Tobacco plants were kept under high W (~200 µmol m^{-2} s^{-1}) for 3 days after agroinfiltration and then leaf circles were treated with W+FR (R:FR, 0.2) and CHX. Relative HFR1 protein levels (ChHFR1, blue bars; AtHFR1, red bars), normalized to the GFP levels, are the means ± SE of four biological replicates relative to data point 0, taken as 1 for each line. Asterisks mark significant differences (2-way ANOVA: * p-value <0.05) between ChHFR1 and AtHFR1 at the same time point.

Figure 5. AtHFR1 interacts more strongly than ChHFR1 with the WD40 domain of COP1.

A Overview of the COP1 WD40-AtHFR1 complex (PDB ID 6QTV). The COP1 WD40 domain and the AtHFR1 VP peptide are shown in surface representation and colored in blue and orange, respectively. The N-terminus of HFR1 VP peptide, the amino acid of which differs between AtHFR1 and ChHFR1, is highlighted in magenta.

B Table summaries of the microscale thermophoresis binding assay (see **Fig EV5**). The sequence of the respective synthetic peptides is indicated.

C Cartoon of constructs containing *ChHFR1*, *AtHFR1*, *ChHFR1** and *AtHFR1** derivatives under the *35S* promoter used for transient expression of transgenes in *N. benthamiana* leaves.

D Relative HFR1 protein levels, normalized to the GFP levels, are the means ± SE of four independent biological replicates. Asterisks mark significant differences (Student *t*-test: * p-value <0.05, ** p-value <0.01) between the indicated pairs.

Figure 6. AtHFR1 interacts with AtPIF7.

A Y2H growth assay showing the interaction between AtHFR1 and AtPIF7. The BD- and the AD- derivative constructs used in the assay are shown on the left side of the panel. SD-LW or SD-HLW refer to the selective medium (plated as drops in dilutions of 1, 1:10 and 1:100) indicative of transformed cells or interaction between the hybrid proteins, respectively. Truncated forms of murine p53 (BD-fused) and SV40 large T-antigen (AD-fused), known to interact, were used as a positive control. Empty vectors (/) were used as negative controls.

B, C Hypocotyl length of seedlings of At^{WT}, **(B)** *pif7-1*, *hfr1-5*, *pif7-1 hfr1-5* (top graph), *pif7-2, hfr1-5* and *pif7-2 hfr1-5* (bottom graph) mutants, and **(C)** transgenic 35S:GFP-ΔNt-HFR1 (35S:ΔNt-HFR1), two lines of 35S:PIF7-CFP (35S:PIF7 #1 and #2), and 35S:GFP-ΔNt-HFR1 35S:PIF7-CFP double transgenic (35S:ΔNt-HFR1 x 35S:PIF7 #1 and #2) seedlings grown under different R:FR. Seedlings were grown in W (R:FR > 1.5) for 7 days or for 2 days in W and then transferred to two W+FR treatments (R:FR 0.06 or 0.02) for 5 additional days. Values of hypocotyl length are the means ± SE of three independent biological replicates (at least 10 seedlings per replica).

D Aspect of representative 7-day-old W-grown seedlings shown in **C**. Scale bar is 1 cm.

Figure 7. *C. hirsuta* has an attenuated hypocotyl elongation at warm temperature and delayed dark-induced senescence (DIS).

A In At^{WT}, PIFs promote hypocotyl elongation as a response to warm temperature (28ºC). High ChHFR1 activity is expected to inhibit this response by repressing PIFs more effectively in Ch^{WT} and attenuate hypocotyl elongation at 28ºC.

B Seedlings were grown for 7 days in W at either 22ºC, 2 days at 22ºC then transferred to 28ºC for additional 5 days (22ºC > 28ºC) or for 7 days at 28ºC, as represented in the panel.

C Hypocotyl length of seedlings of (left) At^{WT}, *pifq*, *pif7-2*, Ch^{WT}, (middle) 35S:GFP-ΔNt-HFR1 (ΔNtHFR1), *hfr1-5* and (right) *chfr1-1* and *chfr1-2* lines grown at warm temperatures. Hypocotyl lengths are the means ± SE of three biological replicates. Asterisks mark significant differences (Student *t*-test: * p-value <0.05, ** p-value <0.01) relative to the same genotype grown at 22ºC (left and right graphs, black asterisks), and between the indicated pairs (middle graph, red asterisks).

D In At^{WT}, PIF-mediated DIS involves a reduction of chlorophyll levels. HFR1 activity might inhibit DIS through repression of PIFs. If PIF activity is attenuated in Ch^{WT}, DIS would be delayed in this species compared to At^{WT}.

E Seedlings were grown for 7 days in W and then transferred to total darkness for several days to induce senescence, as illustrated at the right panel.

F Relative chlorophylls levels of (left) At^{WT}, *pifq*, Ch^{WT}, (middle) ΔNtHFR1, *hfr1-5* and (right) *chfr1-1* and *chfr1-2* lines after DIS was promoted for the indicated time. For each genotype, values are relative to pigment levels at time 0 (7 days in W). Data are the means ± SE of four independent biological replicates.

G Aspect of 4-day old dark-grown seedlings of At^{WT}, *pifq*, *pif7-2*, *hfr1-5* and ΔNt-HFR1 (left panel), and At^{WT}, Ch^{WT} and *chfr1-1* (right panel).

Figure 8. Model summarizing how PIF-HFR1 transcriptional module is differently balanced in *A. thaliana* and *C. hirsuta*.

Shade (low R:FR) displaces phytochrome photoequilibrium towards the inactive form, allowing PIFs to promote the expression of shade avoidance related genes, such as *HFR1*. PIF transcript or/and protein levels are induced in response to warm temperatures, resulting in enhanced expression of growth-promoting genes. HFR1 abundance is also increased by warm temperature. HFR1 modulates these responses by heterodimerizing with PIFs and inhibiting their DNA-binding ability. As a result, HFR1 attenuates hypocotyl elongation of *A. thaliana* seedlings in response to shade or warm temperature. In *C. hirsuta*, higher HFR1 activity inhibits more effectively PIF action than in *A. thaliana*. In addition, PIF abundance is attenuated in *C. hirsuta*. Both changes alter the PIF-HFR1 balance in *C. hirsuta*, resulting in lower PIF transcriptional activity. As a consequence, shade- and warm temperature-induced hypocotyl elongation are repressed and DIS is delayed in this species.

EXPANDED VIEW FIGURE LEGENDS

Figure EV1. Characterization of RNAi-HFR1 and *chfr1* mutants in *C. hirsuta*.

A, **B** Relative expression levels of *ChHFR1* gene, normalized to *EF1α* in Ch^{WT}, **(A)** two RNAi-HFR1 lines (#01 and #21) and **(B)** the two *chfr1* mutants of *C. hirsuta.* Seedlings were grown for 7 days in W. Expression values are the mean ± SE of three independent biological replicates relative to Ch^{WT}. Asterisks mark significant differences (Student *t*-test: ** p-value <0.01) relative to Ch^{WT}.

C The two identified *chfr1-1* and *chfr1-2* mutants have one nucleotide insertion at position 420 of the *ChHFR1* ORF, which leads to a frame shift and a premature stop codon.

Figure EV2. Alignments of *HFR1*, *PIF4*, *PIF5* and *PIF7* partial DNA sequences in *A. thaliana* and *C. hirsuta*

A Location of shared primers and amplicons used for comparison of expression levels by RT-qPCR between species.

B Transcript abundance of *PIF4* and *PIF5*, normalized to *YLS8*, *SPC25* and *EF1α* in Ch^{WT} and At^{WT} grown as in **Fig 2**. Expression values are the means ± SE of three independent biological replicates relative to the data of At^{WT} grown in continuous W at day 3. Asterisks mark significant differences (2-way ANOVA: ** p-value <0.01, *** p-value <0.001) between Ch^{WT} and At^{WT} when grown under W (black asterisks) or W+FR (red asterisks).

Figure EV3. *ChHFR1* and *AtHFR1* complement the *A. thaliana hfr1-5* mutant long hypocotyl phenotype.

A Cartoon of *HFR1* promoters from *A. thaliana* (*pAtHFR1*) and *C. hirsuta* (*pChHFR1*). These promoters cover 2000 bp from the beginning of the translation start of the two *HFR1* genes. The positions of G-boxes (CACGTG) are indicated with arrows.

B GUS staining of representative *A. thaliana* seedlings expressing *GUS* under the *pAtHFR1* (line #03). Seven-day-old W-grown seedlings were treated with W+FR for the indicated amount of time.

C Correlation between Hyp_{W+FR}-Hyp_{W} (means ± SE of at least four biological replicates, data shown in **Fig 3C**) and relative levels of *ChHFR1* or *AtHFR1* expression (means ± SE of three biological replicates, data shown in **Fig 3B**). The estimated regression equations and the R^2 values are shown for each plot.

Figure EV4. ChHFR1 protein accumulates in high W.

A Alignment of AtHFR1 and ChHFR1 protein sequences. Putative COP1 interacting motifs, defined in AtHFR1, are highlighted with a light grey box. VP motifs are highlighted with blue letters. Amino acid sequences inside the blue line rectangles correspond to the synthetic AtHFR1, ChHFR1 and At/ChHFR1 VP peptides used in the microscale thermophoresis assays (Appendix Table S3).

B Cartoon representing the light treatments given to seedlings to estimate relative HFR1-3xHA levels. Seedlings grown for 7 d in low W (~20 µmol m^{-2} s^{-1}, R:FR≈6.4) were first moved to high W (~100 µmol m^{-2} s^{-1}, R:FR≈3.9) for 3 h and then either transferred to high W (control) or high W+FR (R:FR≈0.06) for 3 h. Seedling samples were collected at the time points indicated with asterisks.

C Relative HFR1-3xHA protein levels of *hfr1>35S:ChHFR1* seedlings (line #16) grown as indicated in **B**, with a representative immunoblot in a lower panel. Relative protein levels are the mean ± SE of three independent biological replicates relative to the data point of 0 h in high W (0 h W). Asterisks mark significant differences in protein levels (Student *t*-test: ** p-value <0.01; * p-value <0.05) relative to the 0 h W value.

Figure EV5. Microscale thermophoresis (MST) experimental traces and analysis.

A-F Raw MST traces and analysis of AtCOP1 WD40 with different peptides in triplicates (duplicates for At/ChHFR1 VP). The concentration of AtCOP1 WD40 is fixed at 0.15 µM mixed with 16 serially diluted peptide concentrations at 1:1 ratio. Panels **A**, **C** and **E** show the normalized MST traces. The blue box area illustrates the fluorescence before activation of the infrared- (IR-) laser and red box area illustrates average fluorescence after activation of the IR-laser. Average values ± SD (error bars) were subsequently used for fluorescence normalization. k_D fit displaying fraction bound as a function of ligand concentration is shown in adjacent right panels **B**, **D** and **F**.

A Raw MST traces for AtHFR1 (in blue) and ChHFR1 (in light-brown) VP peptides. Individual concentrations that showed slight aggregation or precipitation are shown in gray and were excluded from the k_D fit calculation.

B Fitted data over a concentration range from 0.032 to 500 µM for AtHFR1 VP (blue dots) and 0.032 to 1000 µM for ChHFR1 VP (light-brown dots) were used to derive the corresponding dissociation constant k_D.

C Raw MST traces for At/ChHFR1 VP peptide (in orange). One concentration that showed slight precipitation or aggregation is shown in gray. A concentration range of 0.0154 to 506 µM was used for the At/ChHFR1 VP.

D No k_D was determined, as no binding between COP1 WD40 and the At/ChHFR1 VP peptide (orange dots) was detected.

E A concentration range from 0.0076 to 250 µM for HsTRIB1 (in red) and AtCRY1 (in green) peptides was used. Raw MST traces show no aggregation or precipitation effects during this binding. One AtCRY1 VP outlier is shown in gray.

F The k_D for HsTRIB1 (brown dots) and AtCRY1 (green dots) VP peptides was calculated using the normalized traces.

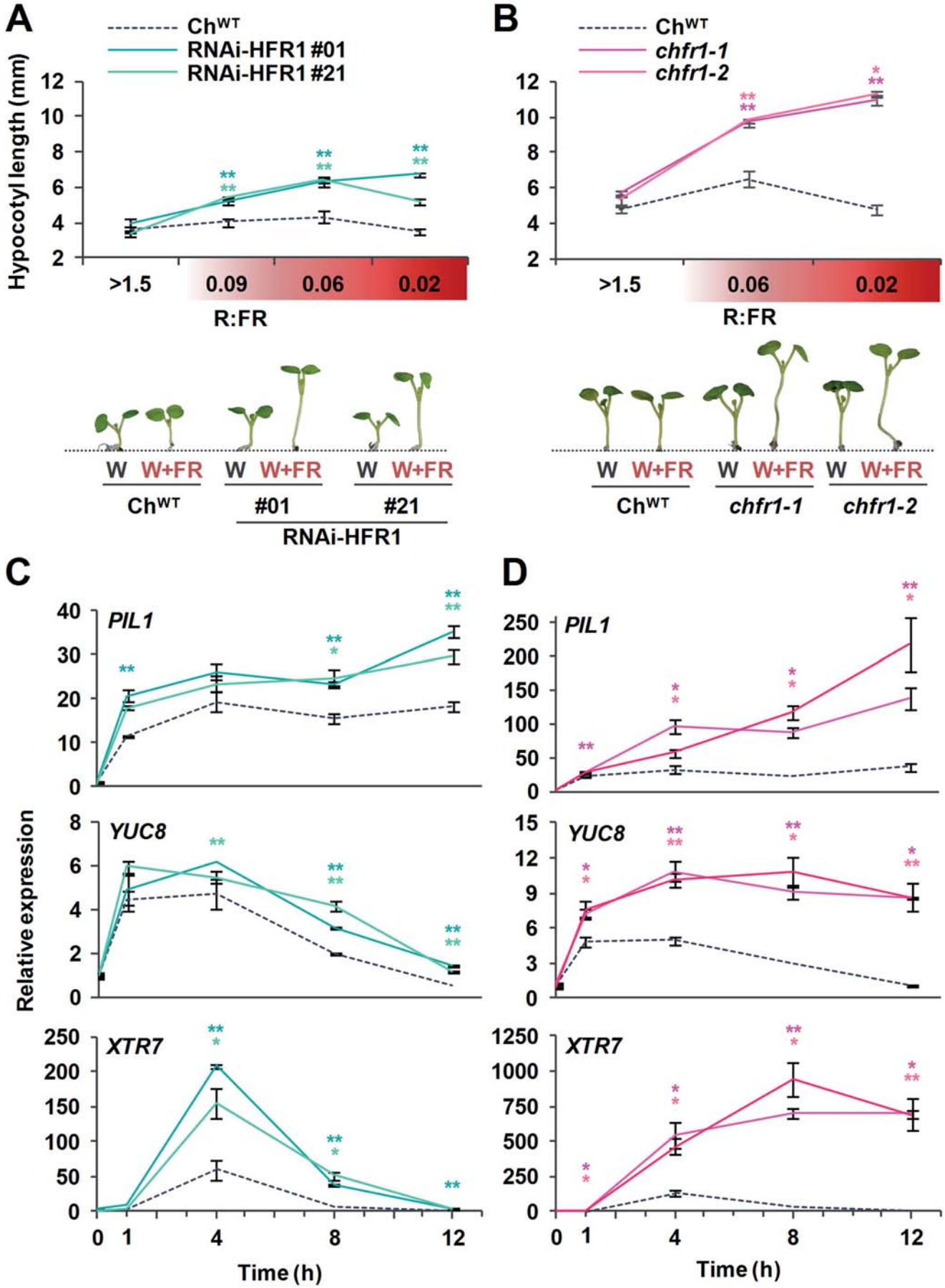
A
Ch^WT
RNAi-HFR1 #01
RNAi-HFR1 #21
Hypocotyl length (mm)
>1.5
0.09
0.06
0.02
R:FR
W
W+FR
Ch^WT
#01
#21
RNAi-HFR1
B
Ch^WT
chfr1-1
chfr1-2
>1.5
0.06
0.02
R:FR
W
W+FR
Ch^WT
chfr1-1
chfr1-2
C
PIL1
YUC8
XTR7
Relative expression
Time (h)
D
PIL1
YUC8
XTR7
Time (h)

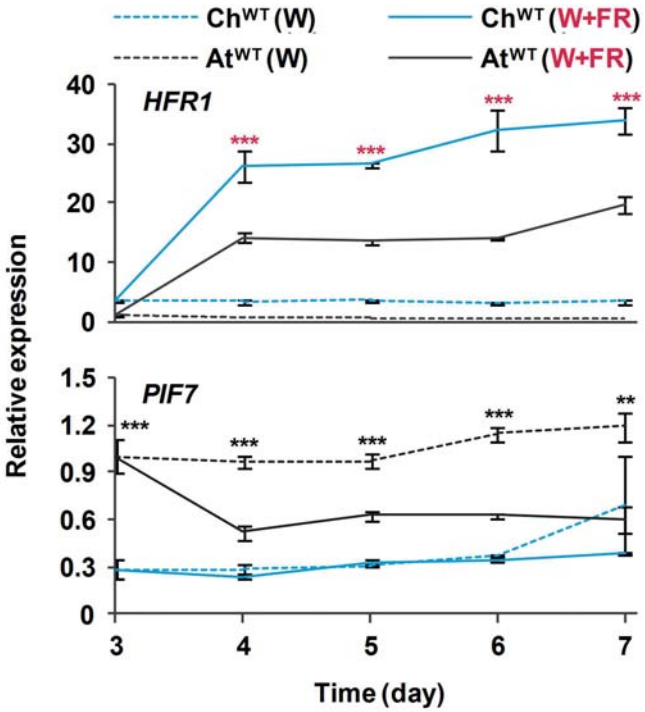
Ch^WT (W)
Ch^WT (W+FR)
At^WT (W)
At^WT (W+FR)
HFR1
PIF7
Relative expression
Time (day)
40
30
20
10
0
1.5
1.2
0.9
0.6
0.3
0
3
4
5
6
7
***
**

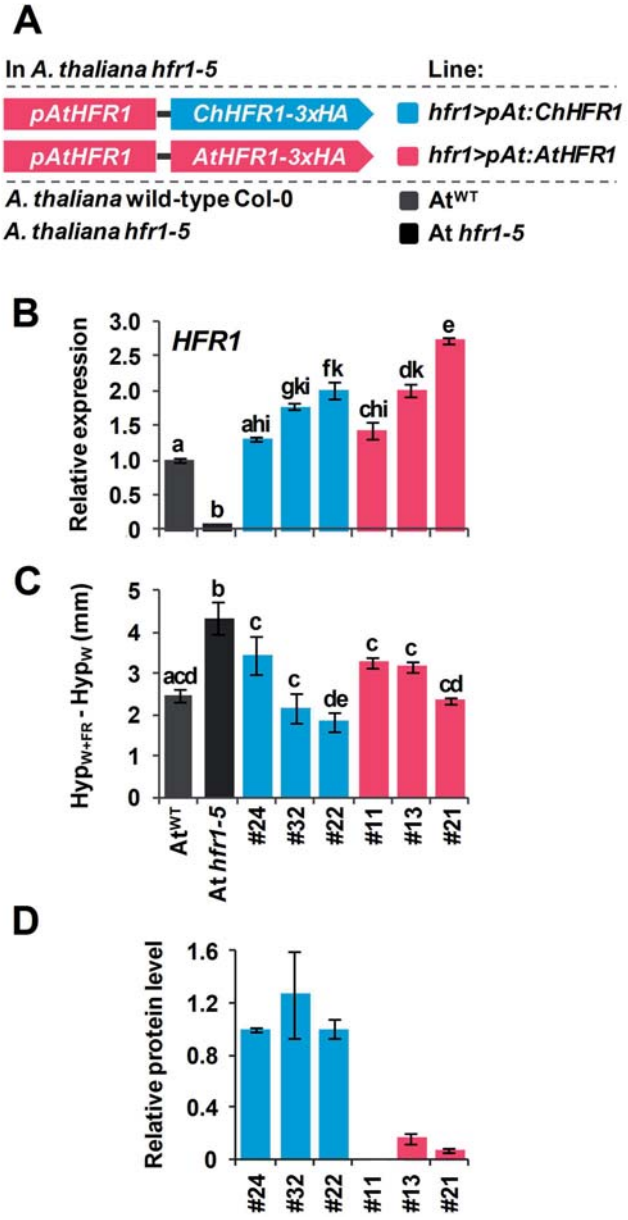
A
In A. thaliana hfr1-5
Line:
pAtHFR1
ChHFR1-3xHA
hfr1>pAt:ChHFR1
pAtHFR1
AtHFR1-3xHA
hfr1>pAt:AtHFR1
A. thaliana wild-type Col-0
AtWT
A. thaliana hfr1-5
At hfr1-5
B
HFR1
Relative expression
3.0
2.5
2.0
1.5
1.0
0.5
0
a
b
ahi
gki
fk
chi
dk
e
C
Hypw+FR - Hypw (mm)
5
4
3
2
1
0
acd
b
c
c
de
c
c
cd
AtWT
At hfr1-5
#24
#32
#22
#11
#13
#21
D
Relative protein level
1.6
1.2
0.8
0.4
0
#24
#32
#22
#11
#13
#21

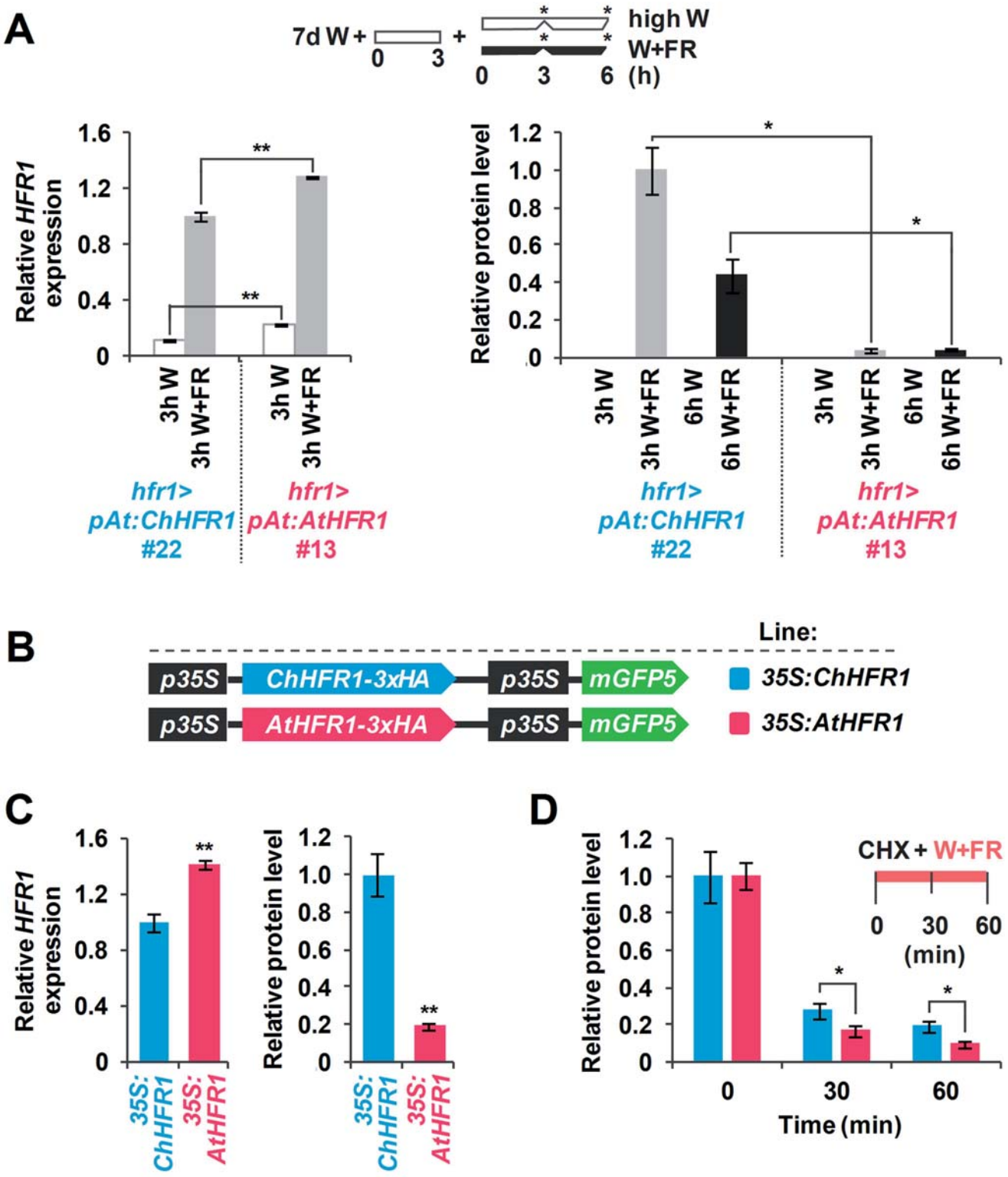
A
7d W +
0
3
+
high W
W+FR
0
3
6
(h)
Relative HFR1 expression
1.6
1.2
0.8
0.4
0
**
**
3h W
3h W+FR
3h W
3h W+FR
hfr1>
pAt:ChHFR1
#22
hfr1>
pAt:AtHFR1
#13
Relative protein level
1.2
1.0
0.8
0.6
0.4
0.2
0
*
*
3h W
3h W+FR
6h W
6h W+FR
3h W
3h W+FR
6h W
6h W+FR
hfr1>
pAt:ChHFR1
#22
hfr1>
pAt:AtHFR1
#13
B
Line:
p35S
ChHFR1-3xHA
p35S
mGFP5
35S:ChHFR1
p35S
AtHFR1-3xHA
p35S
mGFP5
35S:AtHFR1
C
Relative HFR1 expression
1.6
1.2
0.8
0.4
0
**
35S: ChHFR1
35S: AtHFR1
Relative protein level
1.2
1.0
0.8
0.6
0.4
0.2
0
**
35S: ChHFR1
35S: AtHFR1
D
Relative protein level
1.2
1.0
0.8
0.6
0.4
0.2
0
CHX + W+FR
0
30
60
(min)
*
*
0
30
60
Time (min)

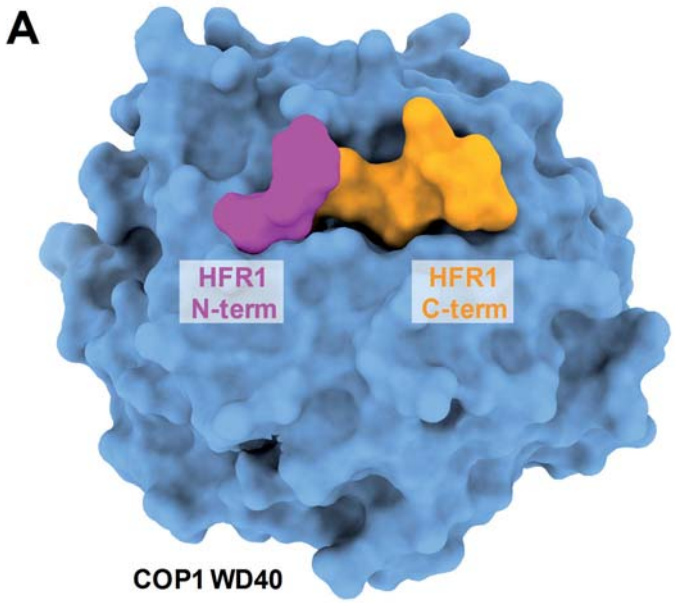

B

Protein	Peptide	k_D
AtHFR1	YLQIVPEI	~ 120 µM
ChHFR1	HHQIVPEI	~ 2 mM
At/ChHFR1	LLVVVPDE	n.d.
AtCRY1	EDQMVPSIT	~ 1 µM
HsTRIB1	SDQIVPE	~ 1 µM

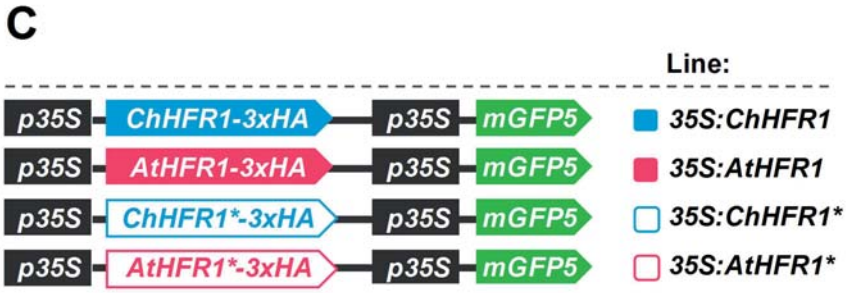

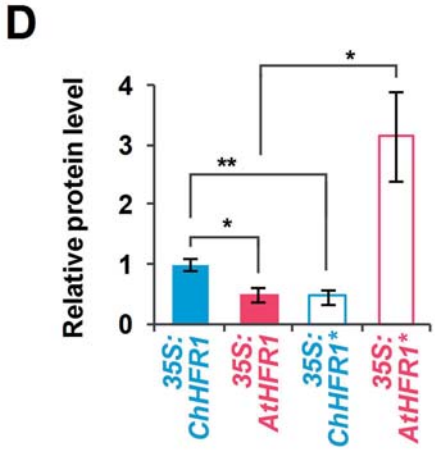

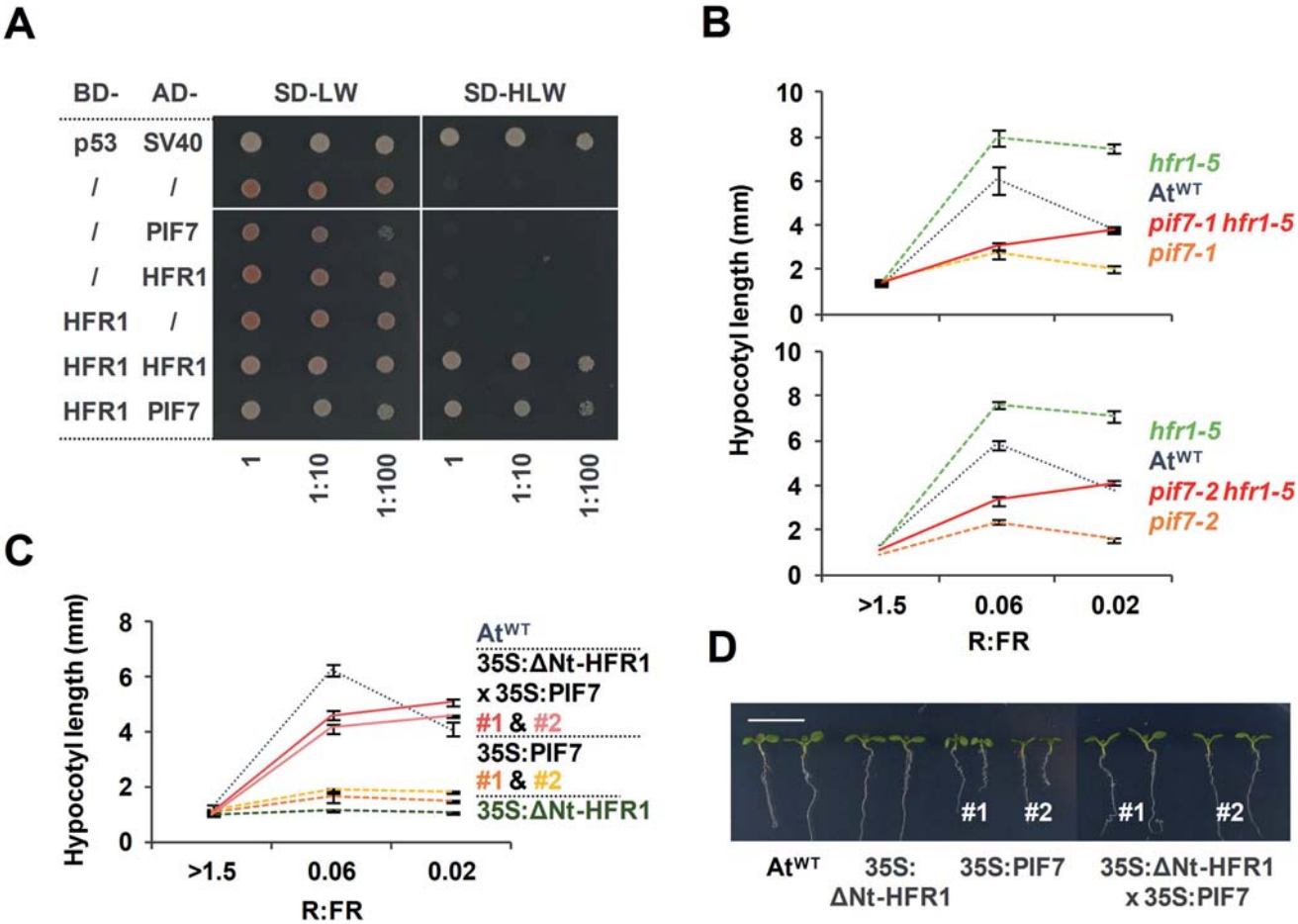
A
BD-
AD-
SD-LW
SD-HLW
p53
SV40
/
/
/
PIF7
/
HFR1
HFR1
/
HFR1
HFR1
HFR1
PIF7
1
1:10
1:100
1
1:10
1:100
B
Hypocotyl length (mm)
hfr1-5
At^WT
pif7-1 hfr1-5
pif7-1
pif7-2 hfr1-5
pif7-2
>1.5
0.06
0.02
R:FR
C
Hypocotyl length (mm)
At^WT
35S:ΔNt-HFR1
x 35S:PIF7
#1 & #2
35S:PIF7
#1 & #2
35S:ΔNt-HFR1
>1.5
0.06
0.02
R:FR
D
#1
#2
#1
#2
At^WT
35S:
ΔNt-HFR1
35S:PIF7
35S:ΔNt-HFR1
x 35S:PIF7

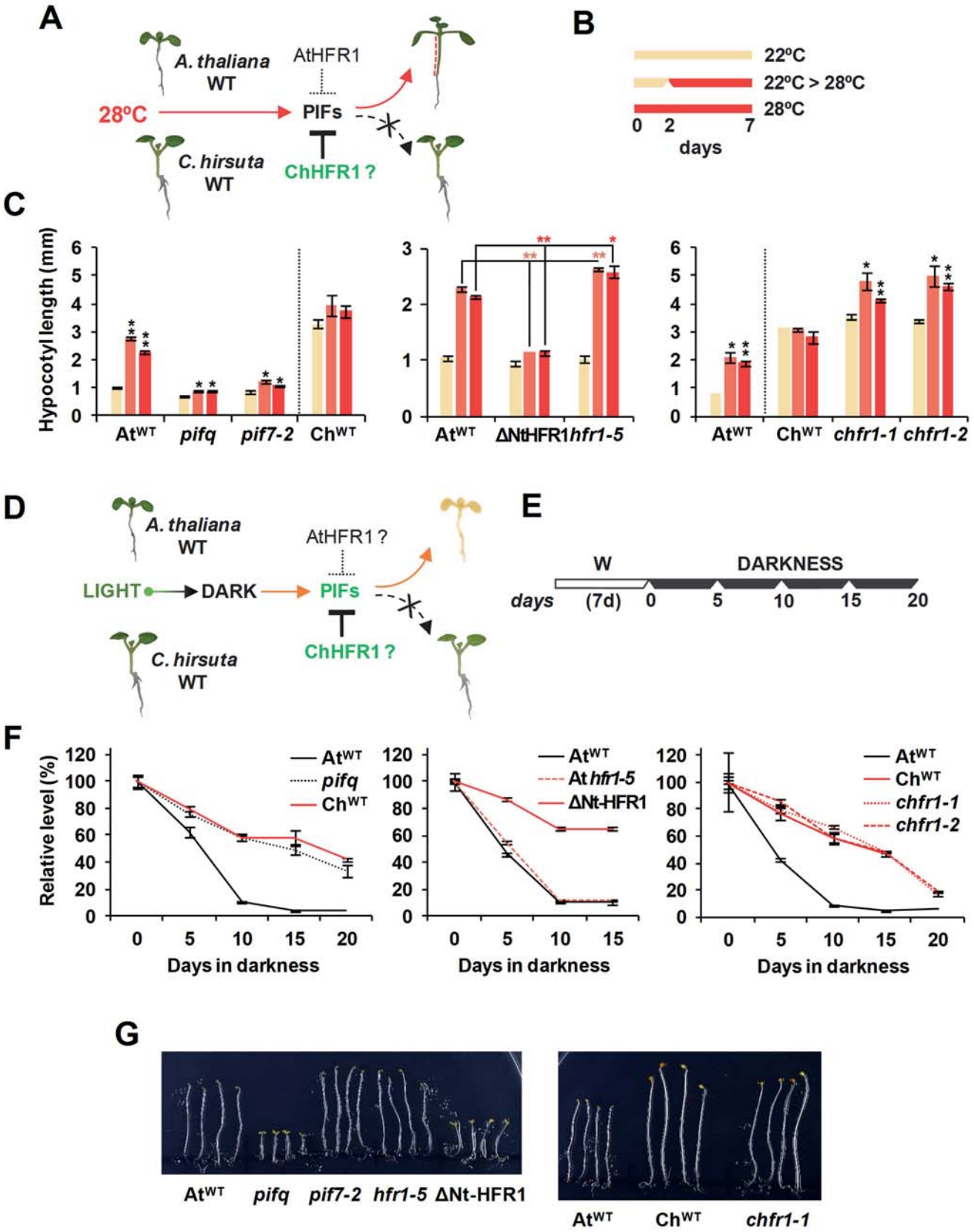
A
A. thaliana
WT
AtHFR1
28ºC
PIFs
C. hirsuta
WT
ChHFR1 ?
B
22ºC
22ºC > 28ºC
28ºC
0 2 7
days
C
Hypocotyl length (mm)
AtWT pifq pif7-2 ChWT
AtWT ΔNtHFR1 hfr1-5
AtWT ChWT chfr1-1 chfr1-2
D
A. thaliana
WT
AtHFR1 ?
LIGHT
DARK
PIFs
C. hirsuta
WT
ChHFR1 ?
E
W
DARKNESS
days
(7d) 0 5 10 15 20
F
Relative level (%)
AtWT
pifq
ChWT
AtWT
At hfr1-5
ΔNt-HFR1
AtWT
ChWT
chfr1-1
chfr1-2
Days in darkness
G
AtWT pifq pif7-2 hfr1-5 ΔNt-HFR1
AtWT ChWT chfr1-1

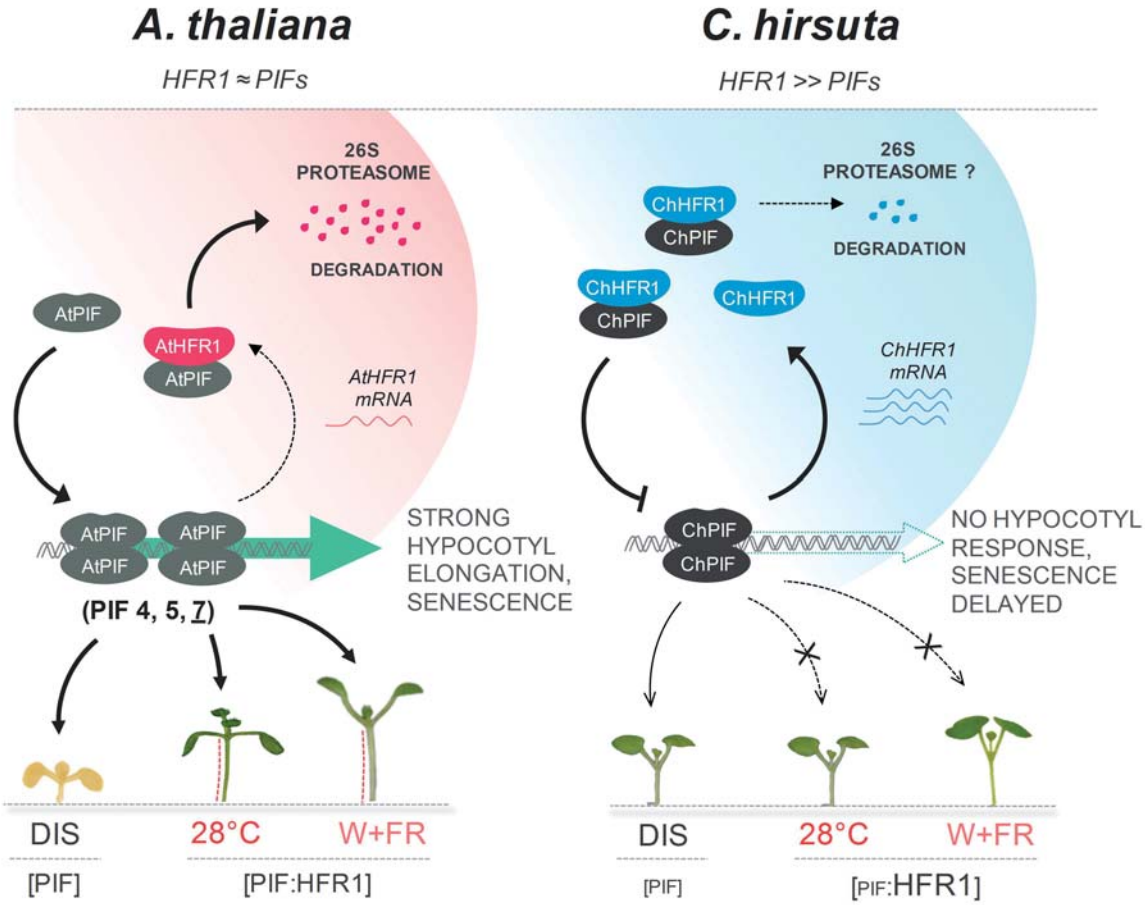
A. thaliana
HFR1 ≈ PIFs
26S PROTEASOME
DEGRADATION
AtPIF
AtHFR1
AtPIF
AtHFR1 mRNA
AtPIF
AtPIF
AtPIF
AtPIF
(PIF 4, 5, 7)
STRONG HYPOCOTYL ELONGATION, SENESCENCE
DIS
28°C
W+FR
[PIF]
[PIF:HFR1]
C. hirsuta
HFR1 >> PIFs
26S PROTEASOME ?
ChHFR1
ChPIF
DEGRADATION
ChHFR1
ChPIF
ChHFR1
ChHFR1 mRNA
ChPIF
ChPIF
NO HYPOCOTYL RESPONSE, SENESCENCE DELAYED
DIS
28°C
W+FR
[PIF]
[PIF:HFR1]

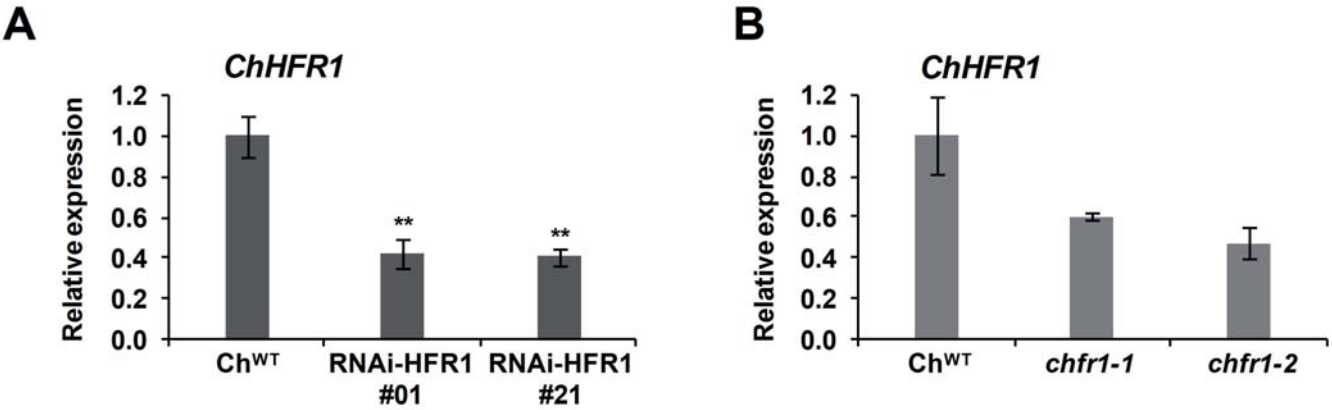
A
ChHFR1
Relative expression
1.2
1.0
0.8
0.6
0.4
0.2
0.0
**
**
ChWT
RNAi-HFR1 #01
RNAi-HFR1 #21
B
ChHFR1
Relative expression
1.2
1.0
0.8
0.6
0.4
0.2
0.0
ChWT
chfr1-1
chfr1-2

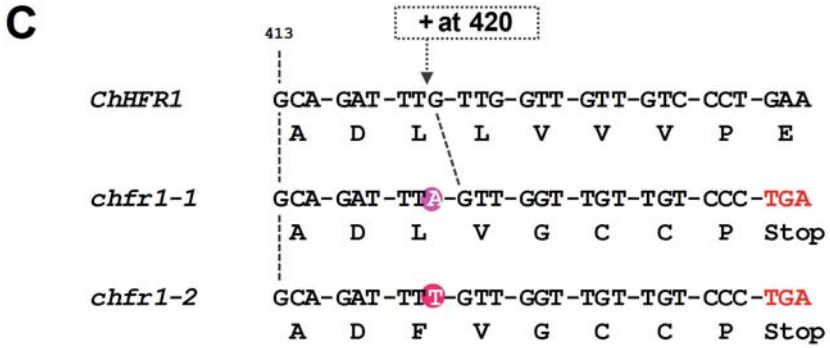
C
413
+ at 420
ChHFR1
GCA-GAT-TTG-TTG-GTT-GTT-GTC-CCT-GAA
A D L L V V V P E
chfr1-1
GCA-GAT-TTA-GTT-GGT-TGT-TGT-CCC-TGA
A D L V G C C P Stop
chfr1-2
GCA-GAT-TTT-GTT-GGT-TGT-TGT-CCC-TGA
A D F V G C C P Stop

A

```
                SPO88                                                                                  SPO89
AtHFR1  TCACCAGCTTCTTCTCCTCAGTCTCTTCACGGTTTGGTTCCTTATTTCCCAAGTTTCTTGGATTTTTCTTCC
ChHFR1  TCGCCAGCTTCTTCTCCTCAATGTCTTTACGGTTTGGTTCCTTGTTTCCCAAGTTTCTTTGATTTTTCTTCC
        **.****************.* ****.**************.************** ************

AtHFR1  CATGCGATGAGA
ChHFR1  CATGCGATGGGA
        *********.**

                SPO108
AtPIF4  GATCCAATACCCTCCAGATGAAGACCCATTCGAACCCGACGACTTCTCCTCCCACTTCTTCTCAACCATGGA
ChPIF4  GATCCAATACCCTCCAGATGAAGACCCATTTGATGCCGACGACTTCTCCTCCCATTTCTTCTCAACCGTTAA
        ****************************.**  ******************.************.* .*

                                SPO109
AtPIF4  TCCCCTCCAGAGACCAACCTCAGAGACGG
ChPIF4  TCCCCTCCAGAGACCAACCTCAGAGATGG
        *************************.**

                SPO110
AtPIF5  ATACATTAATCAGATGGCTATGCAAAGTCAGATGCAATTGTCTCAATTCCCGGTTATGAACCGGTCCGCTCC
ChPIF5  GTTCATTAATCAGATGGCTATGCAGAATCAGATGCAATTGCCTCAATTTCCGGTTATGAACCGGTCCAGTGC
        .* ********************.*.*************.*******.*****************. * *

                                                SPO111
AtPIF5  GCAGAACCATCCCGGTTTAGTATGTCAAAACCCGGTACAGTTGCA
ChPIF5  ACAAAATCATCCCGGTTTAGTATGTCAAAACCCGGTACAGTTCCA
        .**.**.********************************** **

                SPO112
AtPIF7  ATTTCCGCTCTGGATCGGAAACTCAAGATACTGAAGGAGATGAACAAGAGACAAGAGGAGAAGCAGGTAGAT
ChPIF7  ATATCCGCTCTGGATCGGAAACTCAAGATACTGAAGGAGATGAACAAGAGACAAGAGGAGAAGGTGGGAGAT
        ** ************************************************************  ** ****

                                SPO64
AtPIF7  CTAATGGACGACGGGGACGAGCAGCA
ChPIF7  CTAATGGACGACGGGGACGAGCAGCT
        ************************
```

B

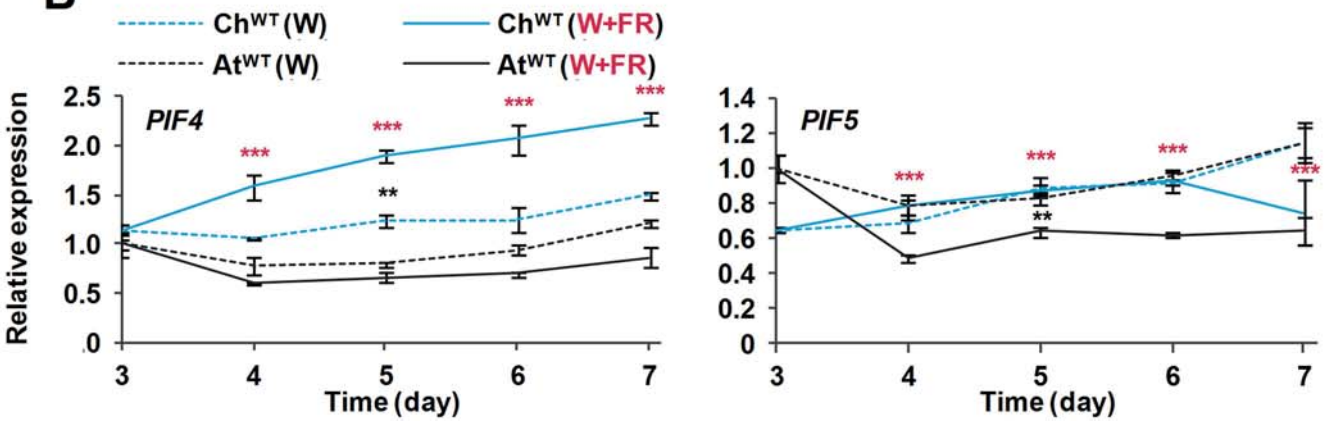

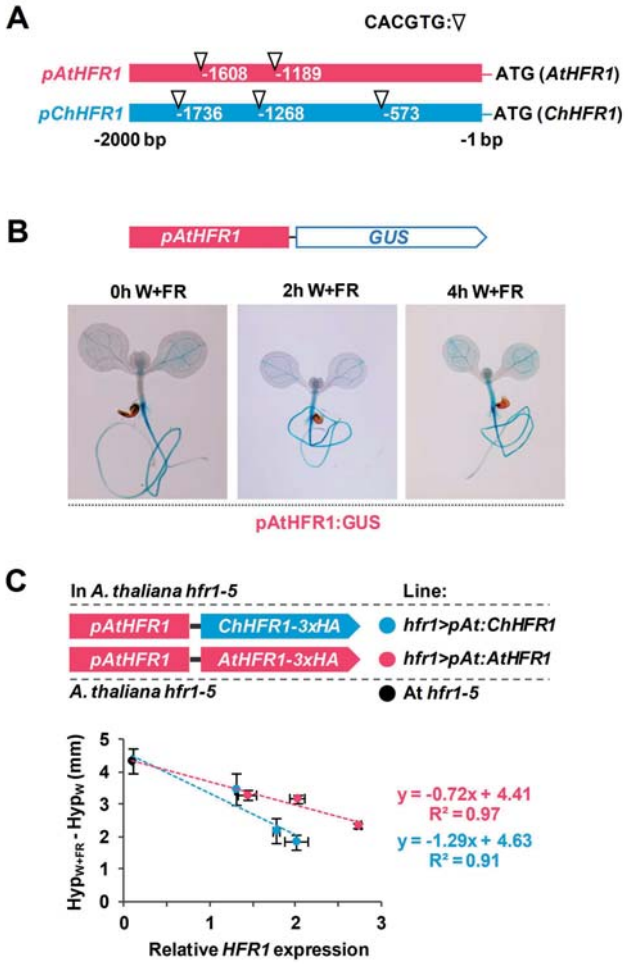
A
CACGTG:▽
pAtHFR1
-1608
-1189
ATG (AtHFR1)
pChHFR1
-1736
-1268
-573
ATG (ChHFR1)
-2000 bp
-1 bp
B
pAtHFR1
GUS
0h W+FR
2h W+FR
4h W+FR
pAtHFR1:GUS
C
In A. thaliana hfr1-5
Line:
pAtHFR1
ChHFR1-3xHA
hfr1>pAt:ChHFR1
pAtHFR1
AtHFR1-3xHA
hfr1>pAt:AtHFR1
A. thaliana hfr1-5
At hfr1-5
HypW+FR - HypW (mm)
Relative HFR1 expression
y = -0.72x + 4.41
R² = 0.97
y = -1.29x + 4.63
R² = 0.91

A

```
AtHFR1 ---------- ---------- ---------- MSNNQAFMEL GWRNDVGSLA VKDQGMMSER ARSDEDRLIN
ChHFR1 MGFPFSRTNL KSPKKNSFLK FSVPDFSLVN MFSNQDFMEL GWRNEVESLA LKDHG-ITDI ARSDEDRLIN
                                        * .** **** ****:* *** :**:* :::  **********

AtHFR1 GLKWGYGYFD HDQTDN-YLQ IVPEIHKEVE NAK-EDLLVV VPDEHSETDD HH--HIKDFS ERSDHRFYLR
ChHFR1 GLKWSYGYFG HDQTHNDHHQ IVPEIQKEER LLKTADLLVV VPDEHSETGD YHHDHIDDYS DSSDNLCYLR
       ****.****. ****.* : * *****:** .   *  ***** ********.* :*  **.*:* : **:  ***

AtHFR1 NKHENPKKRR IQVLSSDDES EEFTREVPSV TRKGS-KRRR RDEKMSNKMR KLQQLVPNCH KTDKVSVLDK
ChHFR1 NKHENPKRRR VQIW-SDEES YGFTREVPSL TRKGSKKRRR RDDELSNKMS TLQELLPNCH KADTVSVLDN
       *******:** :*:  **:**   *******: ***** **** **:::****  .**:*:**** *:*.*****:

AtHFR1 TIEYMKNLQL QLQMMSTVGV NPYFLPATLG FGMHNH-MLT AMASAHGLNP ANHMMPSPLI PALNWPLPPF
ChHFR1 AIEYMKNLQL QLQVMSAMGM NPYFPPATLD FGMSNHYMLT AMALAHIQNP AYQKTSSPLI PASNWPLLPF
       :********* ***:**::*: *********. *** ** *** *** **  ** * :  .**** ** **** **

AtHFR1 TNISFPHSSS QSLFLTTSSP ASSPQSLHGL VPYFPSFLDF SSHAMRRL
ChHFR1 TN-------- -PLFLTTASP ASSPQCLYGL VPCFPSFFDF SSHAMGRL
       **          .*****:** *****.*:** ** ****:** ***** **
```

B

C

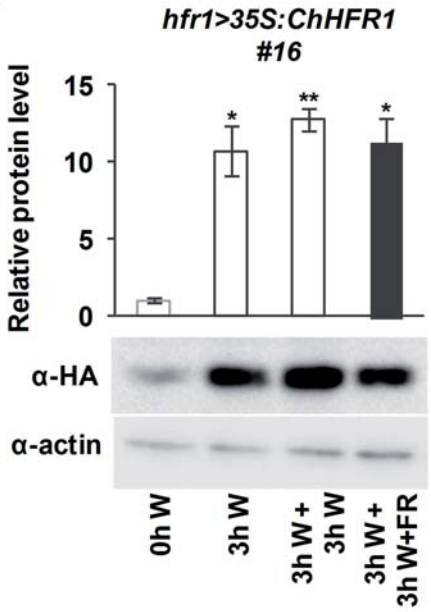

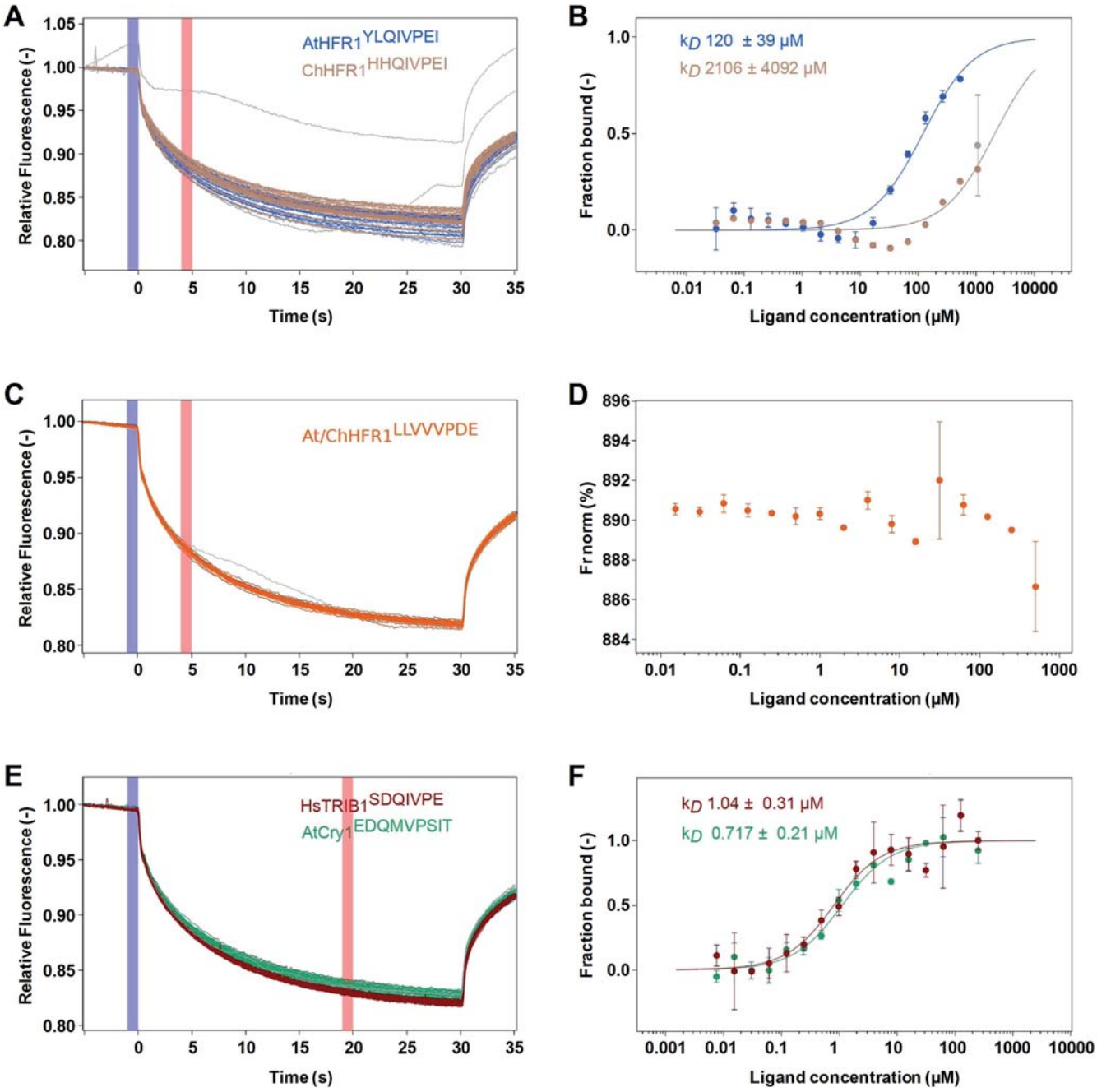
A
AtHFR1YLQIVPEI
ChHFR1HHQIVPEI
Relative Fluorescence (-)
Time (s)
B
kD 120 ± 39 µM
kD 2106 ± 4092 µM
Fraction bound (-)
Ligand concentration (µM)
C
At/ChHFR1LLVVVPDE
Relative Fluorescence (-)
Time (s)
D
Fnorm (%)
Ligand concentration (µM)
E
HsTRIB1SDQIVPE
AtCry1EDQMVPSIT
Relative Fluorescence (-)
Time (s)
F
kD 1.04 ± 0.31 µM
kD 0.717 ± 0.21 µM
Fraction bound (-)
Ligand concentration (µM)

APPENDIX PDF

Adaptation to plant shade relies on rebalancing the transcriptional activity of the PIF7-HFR1 regulatory module.

Sandi Paulišić, Wenting Qin, Harshul Arora Verasztó, Christiane Then, Benjamin Alary, Fabien Nogue, Miltos Tsiantis, Michael Hothorn, Jaime F. Martínez-García

APPENDIX TABLE OF CONTENTS

1. APPENDIX FIGURE S1.

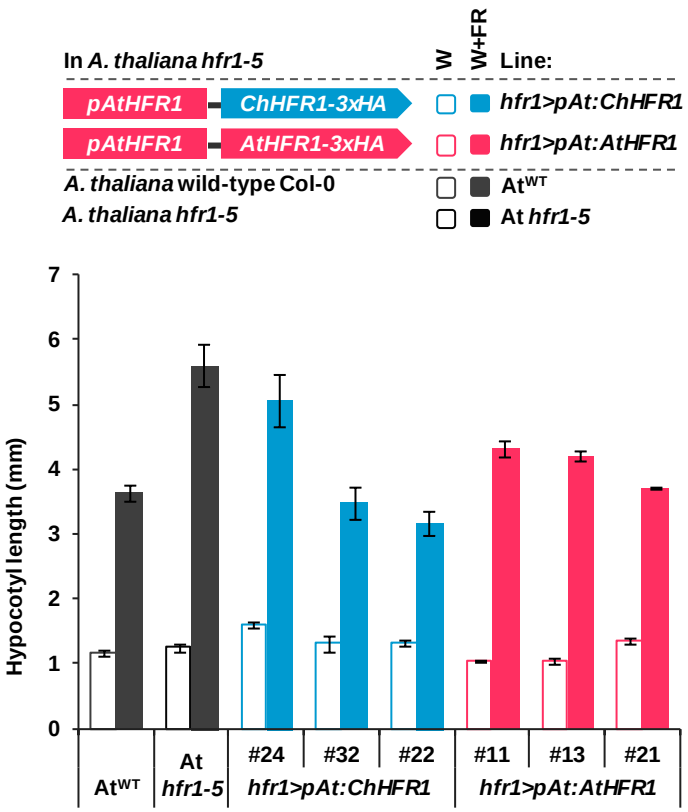

Appendix Figure S1. ChHFR1 and AtHFR1 complement the *A. thaliana hfr1-5* mutant long hypocotyl phenotype. Hypocotyl length of the shown lines grown as indicated in Fig 3C. Values were used to generate data on Fig 3C.

2. APPENDIX FIGURE S2.

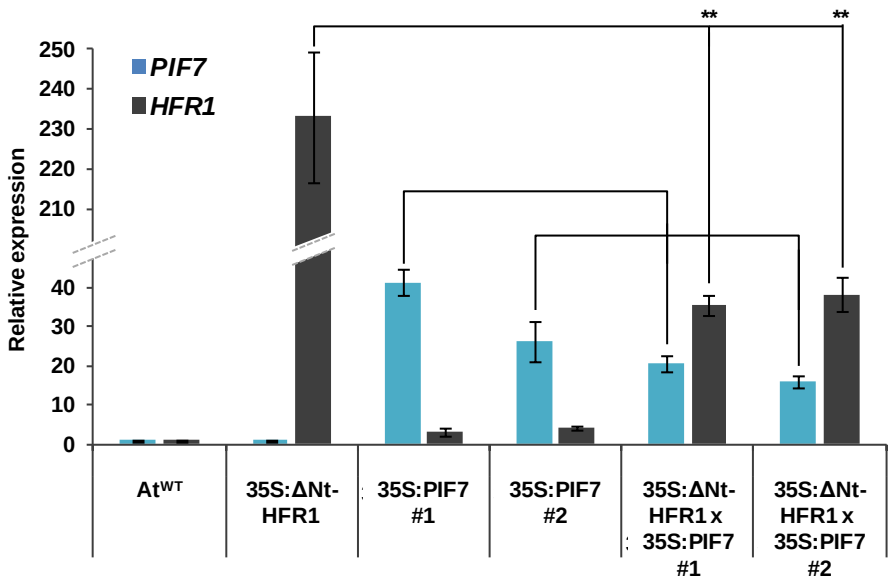

Appendix Figure S2. Relative expression levels of *AtHFR1* and *AtPIF7* genes in transgenic lines overexpressing *GFP-ΔNt-HFR1* and/or *PIF7-CFP*. Relative expression, normalized to *UBQ10*, was estimated in seedlings grown for 7 days in W. Expression values are the mean ± SE of three independent biological replicates relative to At^{WT}. Asterisks mark significant differences in expression (Student *t*-test: ** p-value <0.01; * p-value <0.05) relative to 35S:GFP-ΔNt-HFR1-GFP or 35S:PIF7-CFP values.

3. APPENDIX SUPPLEMENTARY METHODS.

Generation of RNAi-HFR1 plants of *C. hirsuta*

To generate an RNAi construct for silencing of the endogenous *ChHFR1*, a fragment of 222 bp was PCR amplified using primers CTO35 + CTO36 (Appendix Table S2) and cDNA of 7-day old *C. hirsuta* seedlings grown 1 h under W+FR. This partial fragment of *ChHFR1* (ptChHFR1) was cloned into pCRII-TOPO (Invitrogen, www.thermofisher.com) to generate pCT17, which was confirmed by sequencing. An *Eco*RI fragment of pCT17 was subcloned into pENTR3C vector (Invitrogen), to create the Gateway entry clone pCT19 (to have ptChHFR1 flanked with attL1 and attL2, attL1<ptChHFR1<attL2). Recombination of pCT19 with the destination vector pB7GWIWG2(I), which contains attR1 and attR2 sites, using Gateway LR Clonase II (Invitrogen), gave pCT33 (35S:attB1<RNAi-ChHFR1<attB2). This plasmid is a binary vector conferring resistance to the herbicide phosphinothricin (PPT) in plants and the antibiotic spectinomycin in bacteria. *Agrobacterium tumefaciens* strain $C_{58}C_1$ (pGV2260) was transformed with pCT33 by electroporation and colonies were selected on solid YEB medium with rifampicin (100 µg/mL), kanamycin (25 µg/mL) and spectinomycin (100 µg/mL). Wild-type *C. hirsuta* (Ox, Ch^{WT}) plants were transformed by floral dipping and transgenic seedlings were selected on 0.5xGM- medium (Roig-Villanova *et al*, 2006) containing 50 µg/mL PPT. Transgene in seedlings of T1 generation was verified by PCR genotyping using specific primers. Plants homozygous for the transgene were finally used for experiments.

Isolation of *HFR1* mutants of *C. hirsuta*

To obtain loss-of-function mutants of *ChHFR1* in *C. hirsuta* (named as *chfr1*) we employed the CRISPR-Cas9 gene editing system (Morineau *et al*, 2017). The guide RNA targeting ChHFR1 ($gRNA_{ChHFR1}$, 5'-GTT-GAA-GAC-TGC-AGA-TTT-GT-3') was synthesized to be under the control of the *A. thaliana U6* promoter (pU6) sequence and flanked by the Gateway attB1 and attB2 recombination sites (IDT, https://eu.idtdna.com/pages) (attB1<pU6:$gRNA_{ChHFR1}$<attB2). This sequence was recombined with the vector pDONR207 using Gateway BP Clonase II (Invitrogen) to generate the entry vector pSP101 (attL1<pU6:$gRNA_{ChHFR1}$<attL2). In a recombination reaction of pSP101 with pDE-Cas9 (Fauser *et al*, 2014) using Gateway LR Clonase II, a binary vector pSP102 was created (attB1<pU6:$gRNA_{ChHFR1}$<attB2, Cas9). This vector, that contains the information to target ChHFR1, confers resistance to PPT in plants and spectinomycin in bacteria. *A. tumefaciens* strain $C_{58}C_1$ (pGV2260) was transformed with pSP102 by electroporation and colonies were selected on solid YEB medium with antibiotics, as indicated before for pCT33. Wild-type *C. hirsuta* (Ox, Ch^{WT}) plants were transformed by floral dipping and resistant transgenic seedlings were selected on 0.5xGM- medium containing PPT (30 µg/mL). These T1 seedlings were PCR genotyped using primers MJO27 and MJO28 (Appendix Table S2) to detect the presence of the transgene. In the following T2 generation, a total of six seedlings with a *sis* phenotype from 1 independent transgenic line were selected and grown to maturity. An *HFR1* fragment of 664 bp around the $gRNA_{ChHFR1}$ target sequence was amplified by PCR from gDNA of each plant using primers CTO29 + CTO36 (Appendix Table S2). Sequencing of these fragments indicated the presence of

mutations in the *ChHFR1* gene. Descendants of these plants (T3 generation) were reselected in shade and sequenced to confirm the unambiguous presence of the mutated *chfr1* alleles. In the T4 generation, seedlings sensitive to PPT (indicating the loss of T-DNA insertion) were selected, which resulted in the isolation of the *chfr1-1* and *chfr1-2* mutant allele lines (Fig EV1). The wild-type and these mutant alleles were genotyped by PCR using primers SPO104 + SPO107 (for *ChPIF7*), SPO105 + SPO107 (for *chfr1-1*) and SPO106 + SPO107 (for *chfr1-2*) (Appendix Table S2).

Generation of *A. thaliana hfr1-5* transgenic lines expressing *AtHFR1* or *ChHFR1* under the control of different promoters

We amplified a 2 kbp fragment of *AtHFR1* promoter starting immediately before the ATG of *AtHFR1* gene using gDNA of *A. thaliana* wild-type Col-0 (At^{WT}) as a template and primers SPO26 + SPO27 (Appendix Table S2). This fragment was subcloned into pCRII-TOPO to generate pSP51. From the different clones analyzed, the best one was pSP51.10, with three 1 bp-deletions in the amplified region, none affecting the G-boxes, known to be necessary for PIF binding.

AtHFR1 coding sequence was amplified from pJB30 (Galstyan *et al*, 2011) using primers RO25 + SPO30 (Appendix Table S2), which removed the stop codon and introduced a *Xho*I site at the N-terminal site. After subcloning this fragment into pCRII-TOPO, which gave pSP54 (*AtHFR1*), the insert was sequenced to confirm its identity. The 3xHA fragment was amplified from plasmid pEN-R2-3xHA-L3 (Karimi *et al*, 2007) and primers SPO31 (which added a *Sal*I site) + SPO32 (which added a *Xho*I site, Appendix Table S2). This fragment was subcloned into pCRII-

TOPO to generate pSP55 (*3xHA*), whose insert was sequenced to confirm its identity. A *BamH*I-*Xho*I fragment of pSP54 was subcloned into pSP55 digested with *BamH*I and *Sal*I to generate pSP57 (*AtHFR1-3xHA*). A *BamH*I-*Xho*I fragment of pSP57 was subcloned into the same sites of pENTR3C vector which gave pSP59. This plasmid contained *AtHFR1-3xHA*, with an extra *Xba*I site in the C-terminus end, flanked with attL1 and attL2 sites (attL1<*AtHFR1-3xHA*^{XbaI}<attL2). *Xba*I restriction site in pSP59 was removed by filling the site with Klenow enzyme after digestion, and religation to generate pSP84 (attL1<*AtHFR1-3xHA*<attL2). Recombination of pSP84 with the binary vector pIR101 (attR1<*ccdB*<attR2) (Molina-Contreras *et al*, 2019) (using Gateway LR Clonase II) resulted in pSP88 (attB1<*AtHFR1-3xHA*<attB2). An *Xba*I fragment of pSP51 was subcloned into the same site of pSP88 which gave pSP90 (*pAtHFR1*:attB1<*AtHFR1-3xHA*<attB2). This binary vector confers resistance to spectinomycin in bacteria and PPT in plants.

ChHFR1 CDS was amplified using cDNA from wild-type *C. hirsuta* (Ox, Ch^{WT}) seedlings and primers SPO28 + SPO29 (Appendix Table S2), which removed the stop codon and introduced a *Xho*I site. This PCR product was subcloned into pCRII-TOPO to generate pSP53 (*ChHFR1*). Selected colonies were sequenced to confirm their identity. A *BamH*I-*Xho*I fragment of pSP53 was subcloned into pSP55 digested with *BamH*I-*Sal*I to generate pSP56 (*ChHFR1-3xHA*). A *BamH*I-*Xho*I fragment of pSP56 was subcloned into the same site of pENTR3C vector, which gave pSP58. This plasmid contained *ChHFR1-3xHA*, with an *Xba*I site in the C-terminus end, flanked with attL1 and attL2 sites (attL1<*ChHFR1-3xHA*^{XbaI}<attL2). *Xba*I restriction site in pSP58 was removed by

filling the site with Klenow enzyme after digestion, and religation to generate pSP83 (attL1<*ChHFR1-3xHA*<attL2). Recombination of pSP83 with the binary vector pIR101 using Gateway LR Clonase II resulted in pSP87 (attB1<*ChHFR1-3xHA*<attB2). An *Xba*I fragment of pSP51 was subcloned into the same site of pSP87 which gave pSP89 (*pAtHFR1*:attB1<*ChHFR1-3xHA*<attB2). This binary vector confers resistance to spectinomycin in bacteria and PPT in plants.

To overexpress *ChHFR1*, a *BamH*I-*Xho*I fragment of pSP58 was subcloned into the *BamH*I-*Sal*I digested pCAMBIA1300 based pCS14 (Sorin *et al*, 2009) to generate pSP81 (*35S:ChHFR1-3xHA*). This binary vector confers resistance to kanamycin in bacteria and hygromycin in plants.

A. thaliana hfr1-5 plants were transformed with pSP81, pSP89 and pSP90, as previously described. Transgenic seedlings were selected on 0.5xGM- medium with PPT (15 µg/mL) or hygromycin (30 µg/mL), verified by PCR genotyping using specific primers. Homozygous transgenic plants with 1 T-DNA insertion were finally used for experiments.

Generation of constructs for transient expression in *N. benthamiana* leaves

To overexpress *ChHFR1* and *AtHFR1* in *N. benthamiana*, a Gateway vector was created using pCAMBIA1302 (*35S:mGFP5*) as a backbone. An *Nsi*I-*Hind*III fragment of pEarlyGate 100 (*35S*:attR1<*ccdB*<attR2) (Earley *et al*, 2006) was subcloned into pCAMBIA1302 digested with *Pst*I-*Hind*III, which gave pSP135 (*35S*:attR1<*ccdB*<attR2, *35S:mGFP5*). Recombination of pSP58 and pSP59 (both linearized with *Nhe*I) with the binary vector pSP135 using Gateway LR Clonase II gave pSP141 (*35S*:attB1<*ChHFR1-3xHA*<attB2, *35S:mGFP5*) and pSP142

(*35S*:attB1<At*HFR1-3xHA*<attB2, *35S:mGFP5*), respectively. These two binary vectors also overexpress mGFP5 and confer resistance to kanamycin in bacteria.

To generate constructs overexpressing *ChHFR1* and *AtHFR1* with the COP1 binding domains exchanged (Fig 5C), we employed a PCR-based mutagenesis. Using pSP90 as a template, a fragment of 205 bp was amplified with RO25 and SPO126 primers, and a larger fragment of 821 bp was amplified using SPO127 and SPO32 primers. Both PCR fragments were used to amplify *AtHFR1* with the COP1 binding domain from *ChHFR1* (named in here as *AtHFR1**). The resulting fragment was subcloned into pCR8/GW/TOPO (Invitrogen) to generate pSP130, which was confirmed by sequencing. Using pSP89 as a template, a fragment of 291 bp was amplified with SPO28 and SPO128 primers, and a fragment of 800 bp was amplified using SPO129 and SPO32. Both PCR fragments were used to amplify *ChHFR1* with the COP1 binding domain from *AtHFR1* (named in here as *ChHFR1**). The resulting fragment was subcloned into pCR8/GW/TOPO to generate pSP131, which was confirmed by sequencing. Recombination of pSP130 and pSP131 with the binary vector pSP135 using Gateway LR Clonase II gave pSP132 (*35S*:attB1<*AtHFR1*-3xHA*<attB2, *35S:mGFP5*) and pSP133 (*35S*:attB1<*ChHFR1*-3xHA*<attB2, *35S:mGFP5*), respectively. Both vectors also overexpress mGFP5 and confer resistance to kanamycin in bacteria.

N. benthamiana plants were agroinfiltrated with the *A. tumefaciens* (strain GV3101) transformed with pSP141, pSP142, pSP132 or pSP133, and the same strain expressing the HcPro protein (Vilela *et al*, 2013) and kept in the greenhouse under long-day photoperiods. Samples were taken 3 days after agroinfiltration.

Generation of constructs for the Yeast 2 Hybrid (Y2H) assays

AtPIF7 CDS was amplified using cDNA of *A. thaliana* wild-type Col-0 (At^{WT}) seedlings and primers JO414 + JO415 (Appendix Table S2), which removed the STOP codon and introduced a *Xho*I site. This PCR product was subcloned into pCRII-TOPO to generate pRA1 (*AtPIF7*). The insert was sequenced to confirm its identity. A *Xho*I fragment of pRA1 was subcloned into pSP55 digested with *Sal*I to generate pRA2 (*AtPIF7-3xHA*). An *Eco*RI fragment of pRA2 was subcloned into the same site of pENTR3C entry vector which gave pRA3 (attL1<*AtPIF7-3xHA*<attL2). This PIF7-3xHA had a stop codon immediately before the ATG, which prevented from cloning it in frame with the yeast derived proteins. Therefore, the *PIF7-3xHA* gene was PCR amplified using pRA3 as a DNA template and primers BAO4 + BAO5 (Appendix Table S2) to add attB1 and attB2 sequences (attB1<*AtPIF7-3xHA*<attB2). This fragment was recombined with pDONR207 using Gateway BP Clonase II to obtain pBA7 (attL1<*AtPIF7-3xHA*<attL2). The insert was sequenced to confirm its identity. In a recombination reaction of pBA7 and pGBKT7-GW (Chini *et al*, 2009) which contained the Gal4 DNA-binding domain (BD, attR1<ccdB<attL2; it confers Trp auxtrophy), and pBA7 and pGADT7-GW (Chini *et al*, 2009) which contained the Gal4 activation domain (AD, attR1<ccdB<attL2; it confers Leu auxtrophy), using Gateway LR Clonase II, pBA10 (BD-attB1<*AtPIF7-3xHA*<attB2) and pBA11 (AD-attB1<*AtPIF7-3xHA*<attB2) were obtained. These plasmids allowed expressing the fusion BD-PIF7-3xHA or AD-PIF7-3xHA proteins under the *ADH1* promoter in yeast, respectively.

Protein expression and purification for the MST experiments

Sf9 cells were cultured in HyClone SFX-Insect Cell Culture Media. The codon optimized COP1 gene (residues 349-765 corresponding to the WD40 domain) for expression in Sf9 cells, was PCR amplified and cloned into a modified pFastBac (Geneva Biotech) insect cell expression vector using Gibson assembly (Gibson *et al*, 2009). The final construct contained a tandem N-terminal His10-Twin-Strep-tags, a TEV (tobacco etch virus protease) cleavage site prior to COP1 WD40 coding sequence in the pFastBac vector. This construct was transformed into DH10MultiBac cells (Geneva Biotech). White colonies, implying successful recombination, were selected and bacmids were purified by the alkaline lysis method. Sf9 cells were transfected with the bacmid using Profectin (AB Vector). eYFP-positive cells (P0) were observed after 1 week and subjected to two rounds of viral amplification. Sf9 cells at a density of 1–2 x 10^6 cells·ml^{-1} were infected with amplified P2 virus at a Multiplicity of infection (MOI) between 2 to 3. Infected Sf9 cells were grown for 72 h at 28°C and 110 rpm. The cell pellet was then harvested by centrifugation at 2000 x g for 15 min, pellets were flash frozen and stored at –20°C.

Pellets from one liter of Sf9 cell culture were dissolved in 25 ml of buffer A (20 mM HEPES pH 7.5, 300 mM NaCl, 2 mM β-ME), supplemented with 10% [v/v] glycerol, a pinch of DNase, and 1 Roche cOmplete^{TM} protease inhibitor tablet. Dissolved pellets were lysed by sonication and centrifuged at 60,000 x g for 45 minutes at 4°C. The supernatant was consecutively filtered through 2-µm 1-µm and 0.45-µm filters prior to loading onto Ni^{2+}-affinity column (HisTrap excel, GE Healthcare). After the loading, Ni^{2+}-affinity column was washed with buffer A and

eluted directly onto a coupled Strep-Tactin Superflow XT column (IBA) using buffer B (20 mM HEPES pH 7.5, 500 mM NaCl, 500 mM imidazole, 2 mM β-ME). The Strep-Tactin column was washed with buffer A and COP1 was eluted with 1x Buffer BXT (IBA) supplemented with 2 mM β-ME. It was cleaved overnight at 4°C with TEV protease and subsequently purified from the protease and affinity tag by a second Ni^{2+} affinity column. COP1 WD40 was concentrated to 10 μM and was labeled immediately.

GUS lines

Transgenic lines expressing GUS were based on a modified pIR101 plasmid (Molina-Contreras *et al*, 2019) which contains the reporter *GUS* gene in a promoterless context (attB1<*GUS*<attB2). *Xba*I fragment of pSP51 was subcloned into the same site of modified pIR101 to give pSP86 (*pAtHFR1*:attB1<*GUS*<attB2). This binary vector confers resistance to spectinomycin in bacteria and PPT in plants. *A. thaliana* wild-type Col-0 (At^{WT}) plants were transformed with this construct as described previously.

GUS staining

Histochemical GUS assays were done as described (Roig-Villanova *et al*, 2006), incubating seedlings at 37ºC without ferricyanide/ferrocyanide.

<u>4. APPENDIX TABLE S1.</u> Primers used for gene expression analyses. Primers BO40 and BO41 for amplifying *UBQ10* (Sorin *et al*, 2009), SPO102 and SPO103 (*AtEF1α* and *ChEF1α*), SPO113 and SPO114 (*AtSPC25* and *ChSPC25*), and SPO115 and SPO116 (*AtYLS8* and *ChYLS8*) have been described before (Molina-Contreras *et al*, 2019).

Gene	**Primer name**	**Sequence (5' – 3')**
ChEF1α	CTO9 (F)	GGCCGATTGTGCTGTCCTTA
	CTO10 (R)	TCACGGGTCTGACCATCCTTA
ChHFR1	CTO13 (F)	CGGCGTCGTGTCCAGATC
	CTO14 (R)	TGAACCTTTTCGCGTCAGTG
ChPIL1	CTO17 (F)	GAAGACCCCAAAACAACGGTT
	CTO18 (R)	CCCTCATCGTACTCGGTCTCA
ChYUC8	CTO51 (F)	TTACGCCGGGAAAAAAGTTCT
	CTO52 (R)	GCGAAATGGTTGGCTAGGTC
ChXTR7	CTO69 (F)	TGGTGTTCCTTTCCCAAAAAA
	CTO70 (R)	CCACCTCTCGTAGCCCAATC
AtHFR1, ChHFR1	SPO88 (F)	CCAGCTTCTTCTCCTCA
	SPO89 (R)	CATCGCATGGGAAGAAAAATC
AtPIF4, ChPIF4	SPO108 (F)	CCAATACCCTCCAGATGAAGAC
	SPO109 (R)	TCTCTGAGGTTGGTCTCTGG
AtPIF5, ChPIF5	SPO110 (F)	CATTAATCAGATGGCTATGCA
	SPO111 (R)	AACTGTACCGGGTTTTGACA
AtPIF7, ChPIF7	SPO112 (F)	TCCGCTCTGGATCGGAAACTC
	SPO64 (R)	TGCTCGTCCCCGTCGTCCAT
	SPO142 (R)	TCTCATCCTCTGGTTTATCC

5. APPENDIX TABLE S2. Primers used for cloning or/and genotyping. Primer RO25 (Roig-Villanova *et al*, 2007) has been described before.

Gene	Primer name	Sequence (5' – 3')
ChHFR1 WT	SPO104 (F)	CTGTTGAAGACTGCAGATTTG
	SPO107 (R)	CCTAAGGCAAGATTCTTTGAA
chfr1-1 *chfr1-2*	SPO105 (F)	CTGTTGAAGACTGCAGATTA
	SPO106 (F)	CTGTTGAAGACTGCAGATTTT
attB1 attB2	MJO27 (F)	GGGGACAAGTTTGTACAAAAAAGCAGGCT
	MJO28 (R)	GGGGACCACTTTGTACAAGAAAGCTGGGT
pAtHFR1	SPO26 (F)	GCTCTAGAGTAAAGATAACGTTCT
	SPO27 (R)	GCTCTAGAGTTAGTTAAAGAGATA
ChHFR1	SPO28 (F)	CCATGGGTTTTCCATTTTCTCG
	SPO29 (R)	GGCTCGAGGAGTCTTCCCATCGCA
ChHFR1	CTO29 (F)	ATGATCATCATCAAATTGTTC
AtHFR1	RO25 (F)	AACATGTCGAATAATCAAGCTTTCATG
	SPO30 (R)	GGCTCGAGTAGTCTTCTCATCGCA
3xHA	SPO31 (F)	CCGTCGACGGTGGAGGCGGTTCAG
	SPO32 (R)	GGCTCGAGTCAAGCGTAATCTGGA
RNAi-ChHFR1	CTO35 (F)	CAAACACATAATGATCATCATC
	CTO36 (R)	ATCACTCCAGATCTGGACACGA
*ChHFR1**	SPO128 (R)	CTTCTTTATGAATCTCTGGAACAATCTGAAGA TAATTATCTGTTTGATCATGACCAAAA
	SPO129 (F)	GTTCCAGAGATTCATAAAGAAGTAGAAAATGC GAAGGAGGATTTGTTGGTTGTTGTC
*AtHFR1**	SPO126 (R)	CTTTCTGAATCTCTGGAACAATTTGATGATGA TCATTATGAGTTTGATCATGATCAAAG
	SPO127 (F)	GTTCCAGAGATTCAGAAAGAAGAACGACTGTT GAAGACTGCAGATTTATTGGTTGTTGTC
AtPIF7	JO414 (F)	TAACACATGTCGAATTATGGAG
	JO415 (R)	GGCTCGAGATCTCTTTTCTCATGATTC
AtPIF7 + attB1	BAO4 (F)	GGGGACAAGTTTGTACAAAAAAGCAGGCTAC ATGTCGAATTATGGAGTTAAAG
AtPIF7 + attB2	BAO5 (R)	GGGGACCACTTTGTACAAGAAAGCTGGGTGT CAAGCGTAATCTGGAACGTC

6. APPENDIX TABLE S3. Synthetic peptides used for microscale thermophoresis (MST) experiments. The peptides were acetylated (Ac) at the N-terminal and aminated (-NH2) at the C-terminal. The C-terminal tyrosine (Y) residue was added to quantify peptide concentrations via absorbance at 280 nm.

Name	Sequence	Company
AtHFR1 VP	Ac-YLQIVPEI-NH2	Genescript
ChHFR1 VP	Ac-HHQIVPEIY-NH2	Genescript
At/ChHFR1 VP	Ac-LLVVVPDEY-NH2	Genescript
AtCRY1	Ac-EDQMVPSITY-NH2	Peptide Synthesis Laboratory
HsTRIB1	Ac-SDQIVPEY-NH2	Peptide Synthesis Laboratory

7. APPENDIX REFERENCES

Chini A, Fonseca S, Chico JM, Fernandez-Calvo P, Solano R (2009) The ZIM domain mediates homo- and heteromeric interactions between Arabidopsis JAZ proteins. *Plant J* **59:** 77-87

Earley KW, Haag JR, Pontes O, Opper K, Juehne T, Song K, Pikaard CS (2006) Gateway-compatible vectors for plant functional genomics and proteomics. *Plant J* **45:** 616-629

Fauser F, Schiml S, Puchta H (2014) Both CRISPR/Cas-based nucleases and nickases can be used efficiently for genome engineering in Arabidopsis thaliana. *Plant J* **79:** 348-359

Galstyan A, Cifuentes-Esquivel N, Bou-Torrent J, Martinez-Garcia JF (2011) The shade avoidance syndrome in Arabidopsis: a fundamental role for atypical

basic helix-loop-helix proteins as transcriptional cofactors. *Plant J* **66:** 258-267

Gibson DG, Young L, Chuang RY, Venter JC, Hutchison CA, 3rd, Smith HO (2009) Enzymatic assembly of DNA molecules up to several hundred kilobases. *Nat Methods* **6:** 343-345

Karimi M, Depicker A, Hilson P (2007) Recombinational cloning with plant gateway vectors. *Plant Physiol* **145:** 1144-1154

Molina-Contreras MJ, Paulisic S, Then C, Moreno-Romero J, Pastor-Andreu P, Morelli L, Roig-Villanova I, Jenkins H, Hallab A, Gan X *et al* (2019) Photoreceptor Activity Contributes to Contrasting Responses to Shade in Cardamine and Arabidopsis Seedlings. *Plant Cell* **31:** 2649-2663

Morineau C, Bellec Y, Tellier F, Gissot L, Kelemen Z, Nogue F, Faure JD (2017) Selective gene dosage by CRISPR-Cas9 genome editing in hexaploid Camelina sativa. *Plant Biotechnol J* **15:** 729-739

Roig-Villanova I, Bou-Torrent J, Galstyan A, Carretero-Paulet L, Portoles S, Rodriguez-Concepcion M, Martinez-Garcia JF (2007) Interaction of shade avoidance and auxin responses: a role for two novel atypical bHLH proteins. *The EMBO Journal* **26:** 4756-4767

Roig-Villanova I, Bou J, Sorin C, Devlin PF, Martinez-Garcia JF (2006) Identification of primary target genes of phytochrome signaling. Early transcriptional control during shade avoidance responses in Arabidopsis. *Plant Physiol* **141:** 85-96

Sorin C, Salla-Martret M, Bou-Torrent J, Roig-Villanova I, Martinez-Garcia JF (2009) ATHB4, a regulator of shade avoidance, modulates hormone response in Arabidopsis seedlings. *The Plant Journal* **59:** 266-277

Vilela B, Moreno-Cortes A, Rabissi A, Leung J, Pages M, Lumbreras V (2013) The maize OST1 kinase homolog phosphorylates and regulates the maize SNAC1-type transcription factor. *PLoS One* **8:** e58105